

MSAS – Assignment #2: Modeling

Lakrad Adam, 244907

Exercise 1

To perform a preliminary analysis and evaluate a proposed satellite configuration, it is requested to model an active thermal control system and its associated mechanisms to assess the system's capability to maintain the temperatures within a certain range $[T_{min}; T_{max}]$. The satellite body is a rectangular cuboid (1.5 [m] height, 0.5 [m] side), with fixed solar panels (0.5 [m] side, 0.95 [m] length) located on the +Y-axis. The satellite flies with a fixed inertial attitude, with the satellite's Y-axis always directed towards the Sun. The satellite has two extendable radiators, which are located on the $\pm X$ -axis faces. The radiators are connected to the satellite body with electrically controlled hinges that can rotate along the Z-axis direction. The satellite with its radiators in open and closed configurations is represented in Figure 1.

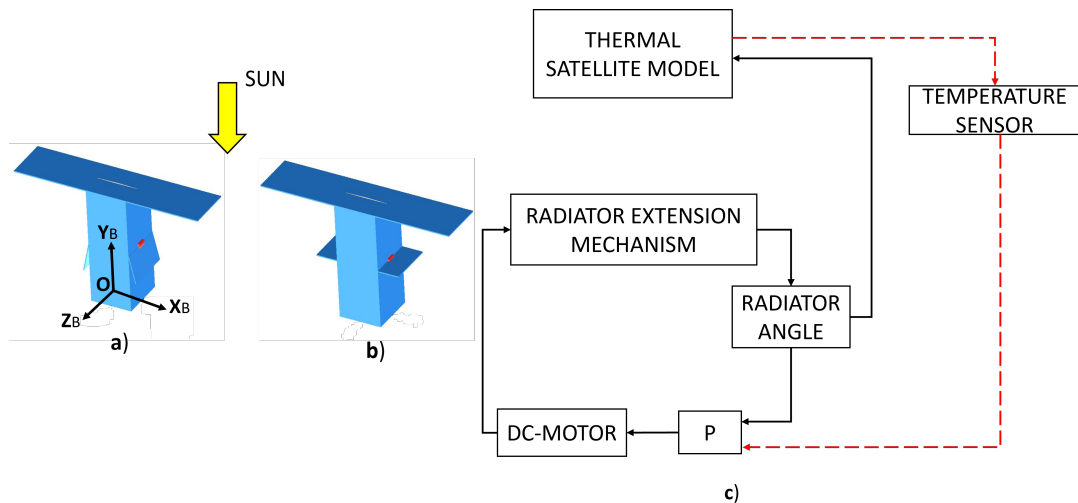


Figure 1: Satellite configuration: **a)** Closed radiator; **b)** Open radiator; **c)** Thermal control logic overview

The extension mechanism is based on a DC motor which gives the needed torque to move the radiator to the desired position. In Figure 2 the physical model of the mechanism is shown. The angle θ represents the rotation of the radiator with respect to the Z-axis and is measured counter-clockwise. For a rotation angle $\theta = 0$ deg, the radiators are in fully open configuration, for $\theta = -0.4\pi$ the radiators are in stowed (closed) configuration. The main parameters of the electro-mechanical model are reported in Table 1.

Parameter	Symbol	Value	Units
Resistance	R	0.1	Ω
Inductance	L	0.001	H
Motor constant	k_m	0.3	Nm/A
Radiator mass	m_r	0.2	kg
Radiator length	L_r	0.5	m

Table 1: Characteristics of the thermal control mechanism.

The radiator has a lower emissivity side, facing deep space in the closed configuration, and a higher emissivity side which is hidden when the radiator is in the stowed position. It is assumed

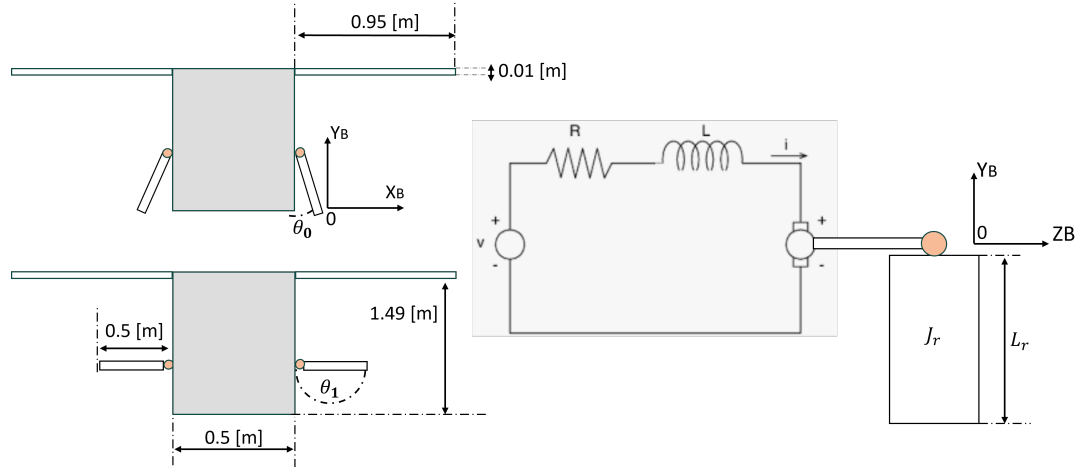


Figure 2: Schematics of the radiator extension mechanism

that radiative heat exchange among the satellite surfaces (re-radiation) is negligible and that no other thermal radiation sources (e.g., planets) are present. As a result, the thermal control of the satellite is regulated mainly by the radiator angle θ , as shown in Figure 1 c). By opening and closing the radiator, the effective area of the high- and low-emissivity sides exposed to deep space increases and decreases respectively. This results in a linear variation of the emissivity ϵ as a function of θ that can be expressed as in Eq. (1):

$$\epsilon(\theta) = \epsilon_{min} + \left[\frac{\epsilon_{max} - \epsilon_{min}}{0.4 \cdot \pi} \right] (\theta(t) + 0.4 \cdot \pi) \quad (1)$$

When the radiator is in a closed configuration with $\theta(t) = -0.4\pi$ [rad] the emissivity is at its minimum $\epsilon_{min} = 0.01$. In fully open configuration instead, when $\theta(t) = 0$ [rad], the radiator emissivity reaches its maximum value $\epsilon_{max} = 0.98$. Using a lumped nodes thermal modeling, the satellite can be divided into 5 components (the two solar panels, the main body, and the two radiators). The radiators and solar panels are connected to the main body node by a conductive path, while all nodes are thermally radiating towards deep space (see Figure 3).

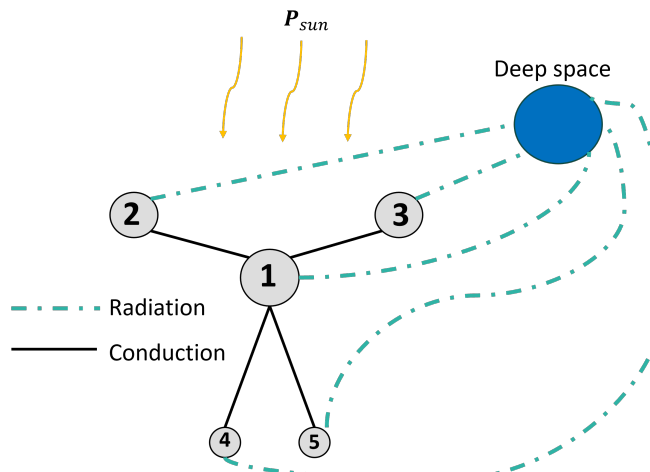


Figure 3: The thermal lumped nodes model

The solar radiation from the Sun is acting only on the two solar panel nodes and on the top face of the main-body node (the radiators are always in shadow). The temperature of deep space is constant and equal to $T_{ds} = 3$ [K]. The characteristics of the thermal network and its components are given in Table 2.



Parameter	Symbol	Value	Unit
Sun Power	P_{Sun}	1350	W/m ²
Heat capacity	C_1	1.5×10^5	J/K
Heat capacity	C_2, C_3	1187.5	J/K
Heat capacity	C_4, C_5	30	J/K
Thermal conductance	$G_{12}, G_{13}, G_{14}, G_{15}$	10	W/K
Absorptivity	α_1	0.6	-
Absorptivity	α_2, α_3	0.78	-
Emissivity	ϵ_1	0.45	-
Emissivity	ϵ_2, ϵ_3	0.75	-

Table 2: Thermal parameters of the system.**Part 1: causal modeling (9 points)**

Considering the following main constitutive equations of the system:

$$C_i \frac{dT_i}{dt} = \sum_i^n (Q_{in}^i - Q_{out}^i) \quad (2)$$

$$V_{in} = k_p \cdot (T_1 - T_1^{ref}) \quad (3)$$

$$J_r \ddot{\theta} = \tau_{in} \quad (4)$$

where Eq. (2) is the conservation of energy at a thermal node; Eq. (6) is a proportional control law in which V_{in} is the input voltage applied on the DC-motor, and T_1^{ref} is the reference temperature of the main-body; and Eq. (4) is the simplified rotational radiator dynamics where the input torque is linked to current flowing into the motor through the relation: $\tau_{in} = k_m \cdot i$. Assuming that: the upper limit \hat{T}_{max} and lower limit temperature \hat{T}_{min} allowed for **node 1** are 300 [K] and 290 [K] respectively, the motor control is capable of maintaining the angle θ within the physical limits, all the thermal nodes start with a temperature of 298.15 [K], and that the radiator is closed at the beginning of the simulation ($\theta(0) = -0.4\pi$):

1. Formulate the full system of non-linear ODEs making explicit the state variables of the whole simulation.
2. Considering a simulation time of at least 50 [h], define the value for the proportional gain k_p such that: the temperature is kept around the target $T_1^{ref} = 294.15$ [K], and within $t = 10$ [h] the maximum temperature oscillations are less than 0.1% of T_1^{ref} . Plot the resulting temperature evolution over time on all thermal nodes.
3. Discuss the results and the ode used in Matlab for the integration.

(9 points)

1. To properly simulate the satellite thermal control system, it is necessary to deconstruct the system, grasping all the underlying physics. The problem is a mixture of three physical domains:
 - Thermal domain, regulating heat transfer within the spacecraft and with external deep space.
 - Mechanical domain, governing the extension mechanism of the radiators.
 - Electrical domain, regulating the DC motor functioning and enforcing the proportional control law.



Assuming negligible re-radiation among satellite surfaces and no thermal sources other than the Sun's heat flux, a system of ODEs governing the heat transfer is established. Using a lumped parameter approach, where each main element is treated as a thermal node, the system consists of three equations due to symmetry. A scheme exposing the thermal system is proposed:

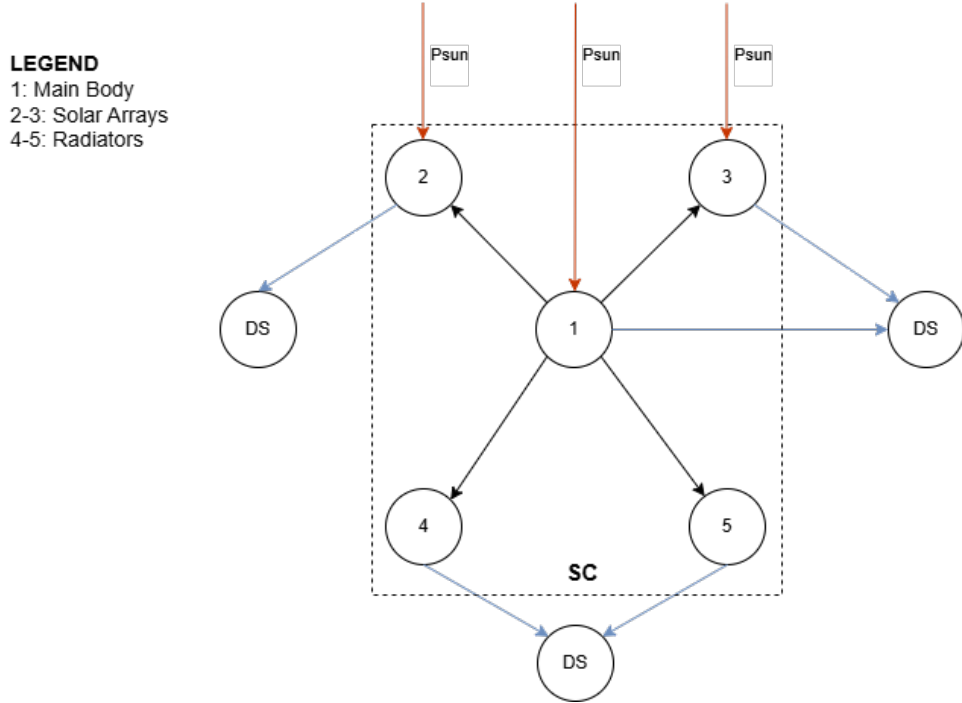


Figure 4: The thermal lumped nodes model.

The thermal lumped model allows to simplify the analysis by considering each main component of the system as a node with a proper equivalent surface. The areas are computed from the data provided by text:

Area	A_1	A_2	A_3	A_4	A_5	$A_{1,Sun}$
Value [m^2]	3.490	0.475	0.475	0.250	0.250	0.250

Table 3: Nodes equivalent surface

Minor surfaces are neglected due to their negligible contribution to the spacecraft's thermal balance. Additionally, since the spacecraft maintains a constant attitude, only the upper surfaces facing the Sun are considered. To simplify the problem, the solar array area exchanging heat with deep space is assumed to be the same as the area absorbing the Sun's heat flux.

Taking Figure 4 as reference ,the heat rate is considered positive when entering the node and negative when exiting from it; using the conservation of energy equation reported above(Equation 2) a system of non linear ODEs is written in the unknowns $[T_1, T_2, T_4]$. The thermal control is enforced in the system thanks to the radiators emissivity, which depends linearly on their angular position with respect to the Z-axis, spacing from a configuration of fully closed radiators ($\theta = -0.4\pi [rad]$) to fully open ($\theta = 0 [rad]$). The radiators opening dynamics is regulated by a DC motor, modelled neglecting any friction and disturbance, whose torque is directly proportional to the current flowing in it.

A closed loop circuit consisting of a voltage generator, a resistor, an inductor and a utiliser is used to model the DC motor.

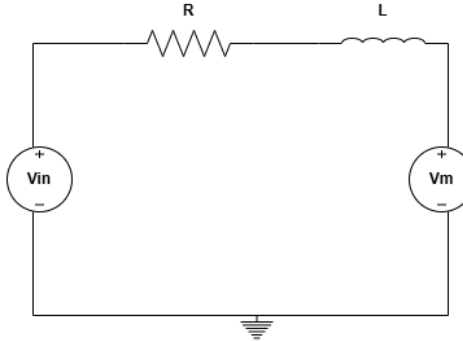


Figure 5: The DC motor circuit.

The voltage drop V_m is proportional to the angular velocity w_m of the radiators, considering the same value as the motor constant k_m . The proportional control law dictates the source voltage, taking into account the difference between the real and the reference temperature of the main body of the spacecraft (node 1 in the model).

Coupling all these domains, the full system of non-linear ODEs is formulated:

$$\left\{ \begin{array}{l} C_1 \frac{dT_1}{dt} = \alpha_1 A_{1,Sun} P_{Sun} - 2G_{12}(T_1 - T_2) - 2G_{14}(T_1 - T_4) - A_1 \epsilon_1 \sigma (T_1^4 - T_{DS}^4) \\ C_2 \frac{dT_2}{dt} = \alpha_2 A_2 P_{Sun} + G_{12}(T_1 - T_2) - A_2 \epsilon_2 \sigma (T_2^4 - T_{DS}^4) \\ C_4 \frac{dT_4}{dt} = G_{14}(T_1 - T_4) - A_{4,tot} \epsilon_4(\theta) \sigma (T_4^4 - T_{DS}^4) \\ \frac{d\theta}{dt} = w_m \\ J_r \frac{dw_m}{dt} = k_m I \\ L \frac{dI}{dt} = -R I - k_m w_m + V_{in} \end{array} \right. \quad (5)$$

The system behaviour is ruled by the following state variables: $[T_1 \ T_2 \ T_4 \ \theta \ w_m \ I]$. The 4th equation is needed to treat the problem as a system of 1st order ODEs. The system is correlated with 2 equations, which enforce the control law and the radiators emissivity dependance on θ :

$$V_{in} = k_p \cdot (T_1 - T_1^{ref}) \quad (6)$$

$$\epsilon(\theta) = \epsilon_{min} + \left[\frac{\epsilon_{max} - \epsilon_{min}}{0.4 \cdot \pi} \right] (\theta(t) + 0.4 \cdot \pi) \quad (7)$$

$$(8)$$

2. In first place, it is necessary to realise a steady state analysis in order to understand if the imposed reference temperature is feasible by the system given or if it is necessary to modify some thermal parameters in order to make it attainable. In this framework, the thermal problem is simply described by the first 3 equations of Equation 5, setting to zero the right-hand side and considering the 2 limit radiator configuration.



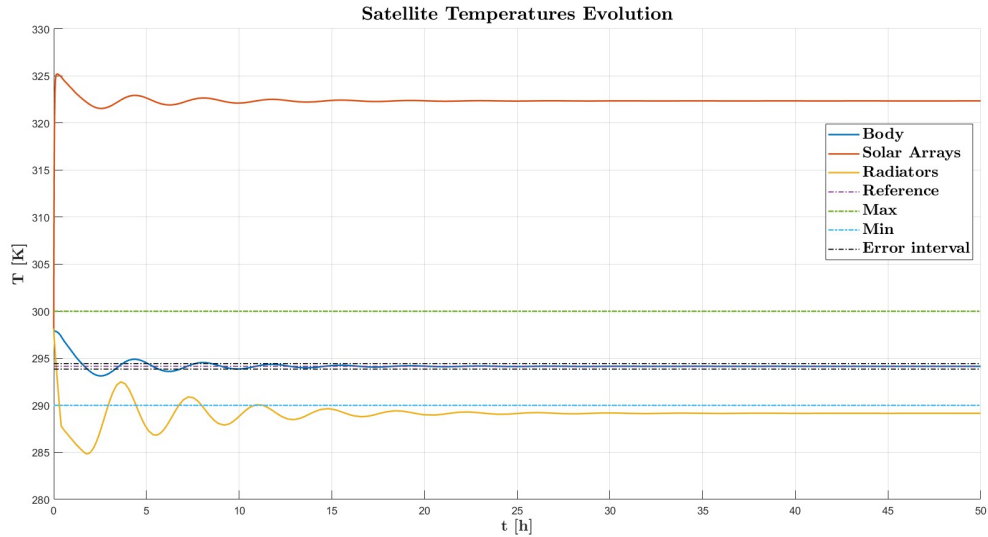
Configuration	T _{body} [K]	T _{SA} [K]	T _{rad} [K]
Closed Radiators ($\theta = -0.4\pi$)	301.2482	327.9103	301.1316
Fully Open Radiators ($\theta = 0$)	288.6788	318.0309	280.1246

Table 4: Steady State Analysis Results for Different Radiator Configurations

Through the use of Matlab build-in function *fsolve*, it is possible to state that the problem is well posed since the reference temperature is in the T_{body} range.

Since in the causal modeling, all the physical and logical constraints should be fully enforced into the mathematical model of the problem, a special focus is posed on the physical behaviour of the radiators' opening mechanism and on its functioning logic. The radiators shall not exceed their physical domain of $[-0.4\pi \text{ rad}; 0 \text{ rad}]$, but also be capable of remaining fully open or closed, depending on the main body temperature. The fully open configuration ($\theta = 0 \text{ rad}$) should be maintained when T_1 is greater than the reference temperature to decrease in the most efficient and rapid way the main body temperature; specularly, the fully closed configuration ($\theta = -0.4 \text{ rad}$) should be maintained when T_1 is lower than the reference temperature to increase the main body temperature. The condition is physically enforced by turning off the DC motor, with the hypothesis that it immediately stops rotating whether the input current is null. Computationally, a conditional expression evaluates the proximity of θ to the interval bounds, taking into account a small tolerance of 10^{-16} rad , coupled with the sign of $T_1 - T_{ref}$, to enforce the rationale exposed above. In both cases where the radiators are in limit configuration, the electrical circuit parameters(I, V_{in}) are set to zero along with the angular velocity of the rotor.

The goal of the simulation is to bring the body temperature T_1 to the reference value within 10 hours and maintain it within a range of 0.1% T_1^{ref} . It is necessary to tune the proportional control constant while considering these requirements, avoiding overly tight constraints to prevent undesired overshooting and increased computational effort. The optimal k_p is determined using a genetic algorithm, an optimization method that simulates natural evolution through selection, crossover, and mutation to find the parameter that minimizes the cost function $J = \frac{1}{n} \sum_{i=1}^n (T_{1,i} - T_{\text{ref},i})^2$, where n represents the number of time steps. The search is restricted to the interval $[10^{-3}; 10^{-6}]$ to avoid reaching the reference temperature any sooner than 10 hours. The resulting temperature evolution over time in all thermal nodes using $k_p = 7.25e - 5$ is the following:

**Figure 6:** Temperature evolution

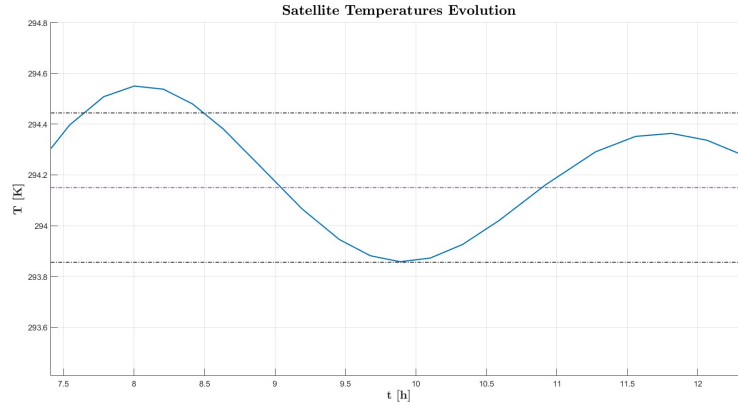
It is straightforward to notice that the main body temperature reaches the imposed reference temperature with a value bounded in the given range. Both the solar arrays and the radiators reach an equilibrium temperature in their limit temperature range, underlying the importance of the preliminary steady-state analysis conducted. In particular, the solar arrays temperature rapidly departs from the initial temperature $T_0 = 298.15\text{ K}$, being particularly different from the reachable equilibrium range; in contrast, the radiators temperature presents a wider oscillation dictated by the high sensitivity on the opening angle and consequently on the emissivity, also due to the absence of constant Sun heat flux for them.

The nodes temperatures after 50 hours are reported in the following Table 5:

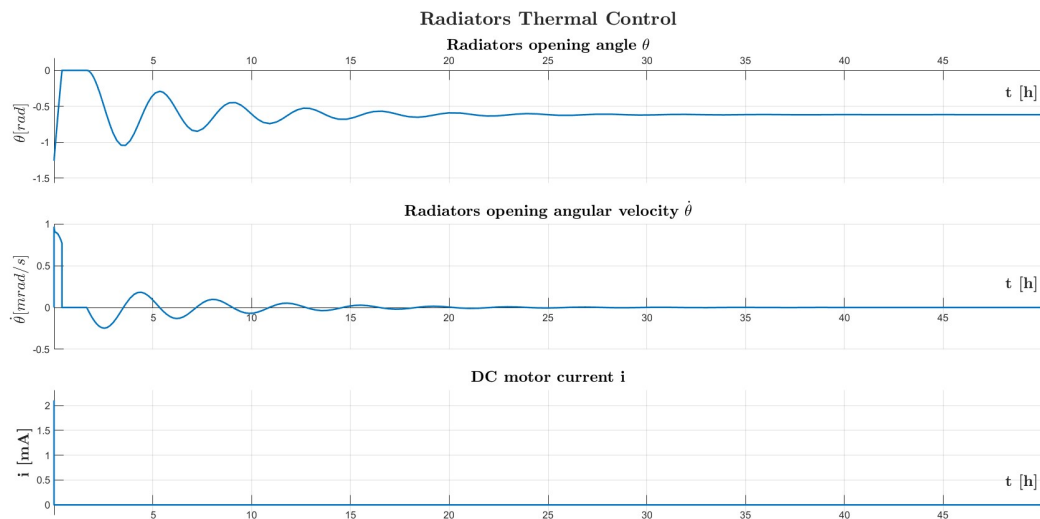
T_{body} [K]	T_{SA} [K]	T_{rad} [K]
294.1503	322.3553	289.1531

Table 5: Nodes temperature after 50 hours

The choice of proportionality control constant is justified by the smooth approach of T_{body} to T_{ref} and by a proper dumping behaviour that allows to enter the maximum oscillations range in approximately 10 hours, as better shown in Figure 7.

**Figure 7:** Zoom on T_1 in 10 hours proximity

The oscillating temperature trend is better justified by the following Figure 8:

**Figure 8:** Radiators electro-mechanical system state variables time evolution

At the beginning of the simulation, the radiators rapidly reach the fully open configuration since, at the initial state, node 1 is hotter than the reference temperature and for $\theta = 0 \text{ rad}$ the emissivity is maximum. As a result, the DC motor is shut down until the temperature decreases below the reference and from that point forward, a fine tuning of the radiators opening is performed in order to let T_{body} converge to T_{ref} .

The current behavior is better observable in Figure 46 and Figure 47, reported in the Appendix.

The spacecraft at first readily cools down and then precisely tune the opening of the radiators until it finds the opening angle $\theta = -0.1962\pi \text{ rad}$ related to $\epsilon_{radiator} = 0.5044$ which accurately allows to maintain the reference temperature.

3. Due to the multi-physical character of the problem, distinguished by different time scales, the integration is performed using *ode23s* allowing to decrease the computational effort alongside with an accurate solution, regardless of the relative small number of points(253) computed in approximately 0.04 s. Non-stiff ode solvers require a much greater compu-



tational, which make them unsuitable for the resolution of this problem and on extension of multi-physical problems.

Part 2: acausal modeling (6 points)

Using the Modelica standard library, reproduce in Dymola the physical model of the thermal-electro-mechanical system described above. You can build your **own model block** in Modelica to implement specific signals such as $\epsilon(\theta)$ or the control strategy. Please note that when you create a new model block (see in Table 6) you can insert input/output variables and your equations (see as an example the **Text View** of the block: *Modelica/Blocks/Math/Add*). Then, simulate it in OpenModelica comparing the results with the ones obtained using the causal model.

<i>Physical element</i>	<i>Modelica library</i>
Rigid-body	Modelica/Mechanics/MultiBody/Parts
Revolute joint	Modelica/Mechanics/MultiBody/Parts
Fixed-translational element	Modelica/Mechanics/MultiBody/Parts
DC-motor	Modelica/Electrical/Machines/BasicMachines/DCMachines
Thermal node	Modelica/Thermal/HeatTransfer/Components
Thermal resistances	Modelica/Thermal/HeatTransfer/Components
Logical switch	Modelica/Blocks/Logical/Switch
Hysteresis	Modelica/Blocks/Logical/Switch
Temperature sensor	Modelica/Thermal/HeatTransfer/Sensors
Your model block	File/New/Block

Table 6: Modelica libraries.

(6 points)

The acausal modeling is particularly suitable to describe multi-physical systems, like the one in analysis. The advantage relies on the possibility of building the model by simply connecting the systems' components, since the mathematical structure of the problem is hidden.

As exposed previously, the problem is characterised by 3 physical domains, which are linked through proper elements.

- Thermal domain

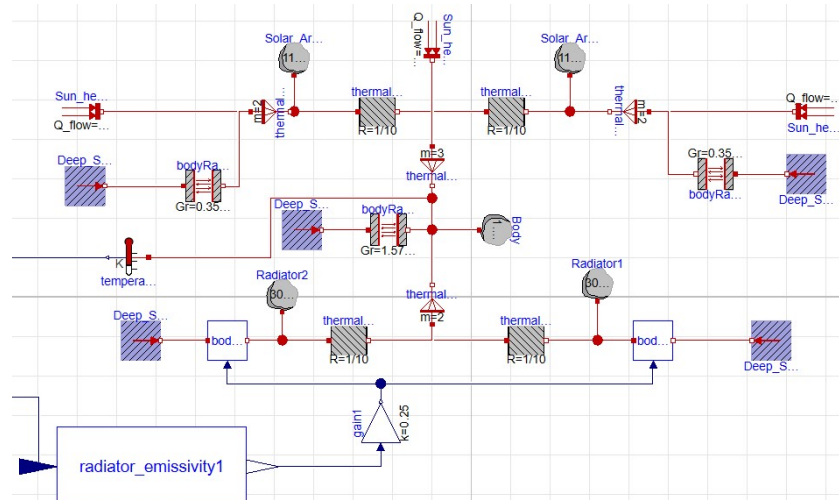


Figure 9: Acausal Model of thermal system



Each node is characterised by a thermal capacity block, which represents its thermal inertia. The thermal flux is modelled through the use of a thermal collector that sums the different heat powers in input and output, taking as heat flux directions the one depicted in Figure 4. The system is validated using a constant radiators emissivity, modeling the steady state case, which gives back the same results of Matlab.

To model the radiators varying emissivity, depending on θ , is necessary to create an ad hoc block, since the build-in "bodyRadiation" block does not account for varying emissivity. The specifically created block allows to take as input the net radiation conductance, besides the temperatures.

As Figure 9 shows, the input emissivity comes from another created block that implements the emissivity relation with θ ; the present gain multiplies the emissivity by the radiator's surface to obtain the required radiation conductance. A temperature sensor is linked to node 1 in order to implement the proportional control logic, based on $T_1 - T_{ref}$.

- Electrical domain

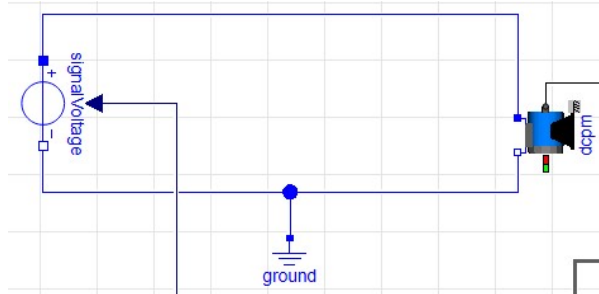


Figure 10: Acausal Model of electrical system

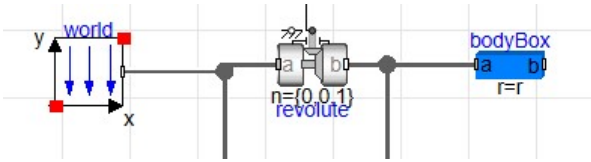
It could appear that the model is simplified since the "Permanent magnet DC machine" model does not require to explicitly model the DC motor inner circuitry, as done for the causal model; however, the parameter settings largely influence the simulation and require a particular fine tuning in order to obtain results close to the one of the causal modeling.

Parameter	Value	Unit	Description
VaNominal	94.25	V	Nominal armature voltage
IaNominal	1	A	Nominal armature current
wNominal	314.159265358793	rad/s	Nominal speed
TaNominal	-	°C	Nominal armature temperature

Table 7: DC motor Dymola nominal parameters

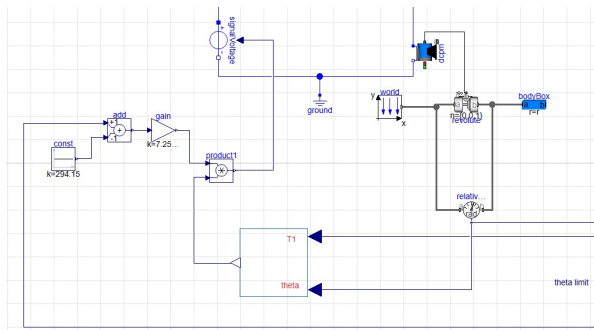
It is noted that the DC motor could be modeled using a resistor, an inductor, and a Dymola "ElectroMechanicalConverter." However, this approach is not aligned with the purpose of acausal modeling, which focuses on modeling complex systems using pre-built blocks that require careful parameter selection. The input voltage is determined by the control logic.

- Mechanical domain

**Figure 11:** Acausal Model of mechanical system

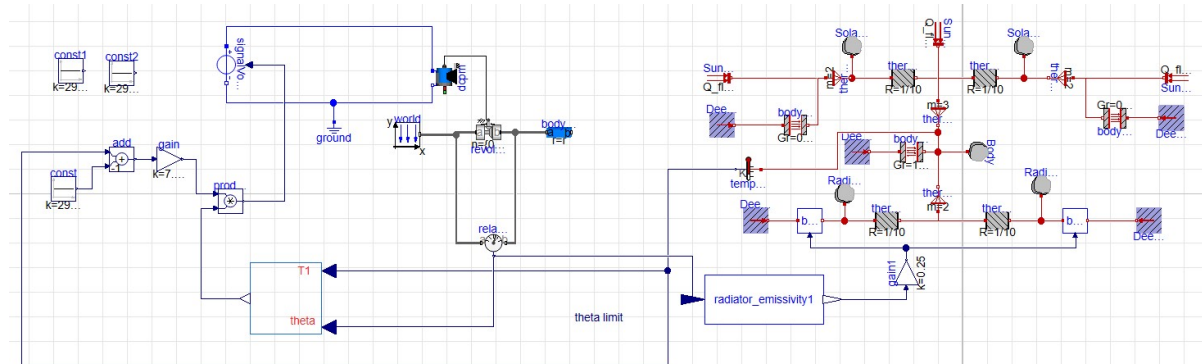
The radiator's opening mechanism is modeled using a revolute joint, which takes the DC motor torque as input and rotates the radiator. The radiator is represented by a Dymola "bodyBox," with parameters precisely set to accurately simulate and visualize the radiator's dynamics through animation. The chosen values are reported in Appendix (Figure 48). An extremely small dimension is chosen in order to model the negligible radiator thickness but still being able to use this block and properly compute the radiators inertia with respect to the axis or rotation.

- Control logic

**Figure 12:** Proportional control logic model

The control logic is implemented using a "LimitBehaviour" block that takes θ and T_1 as inputs. Following the rationale of causal modeling, it outputs either 0 or 1 to directly turn off the DC motor by setting the input voltage to zero in the electrical circuit. If the DC motor needs to be on, the input voltage is regulated by the proportional control law $V_{in} = k_p (T_1 - T_{ref})$. Although the control logic could also be implemented using boolean blocks, this would sacrifice the simplicity typical of acausal modeling. It is noteworthy that the DC motor almost immediately stops generating torque when the applied potential is zero.

The complete model is shown in Figure 13:

**Figure 13:** Complete Dymola acausal model



The simulation is conducted in OpenModelica using 5000 time steps, a tolerance of 1×10^{-6} , and the DASSL (Differential/Algebraic System Solver) due to its capability to handle stiffness and maintain stability. The results are presented in the following plots.

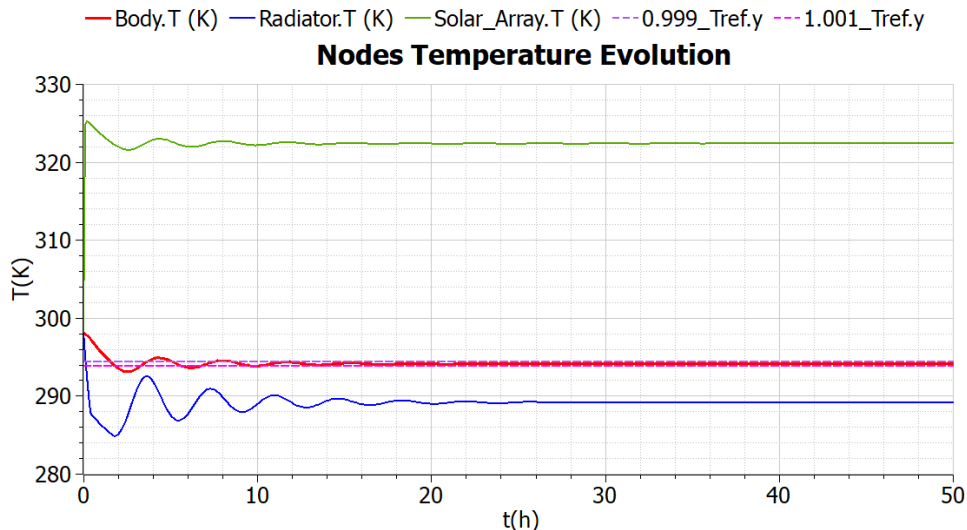


Figure 14: Dymola Temperatures evolution

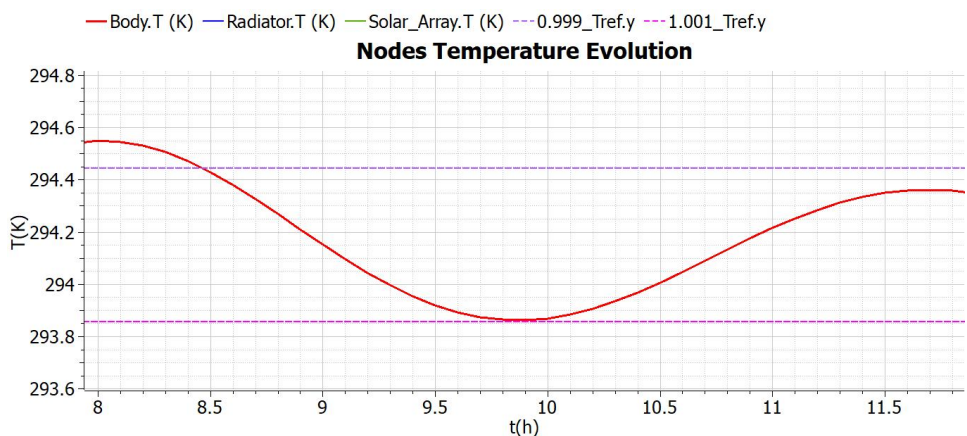


Figure 15: Zoom on T_1 in 10 hours proximity in Dymola

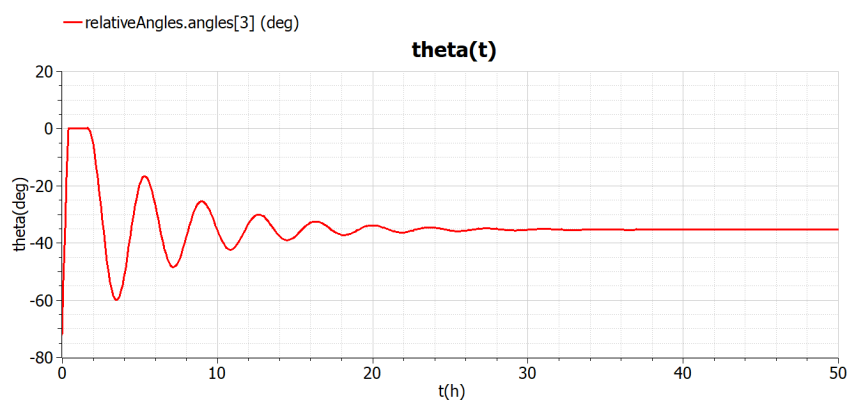
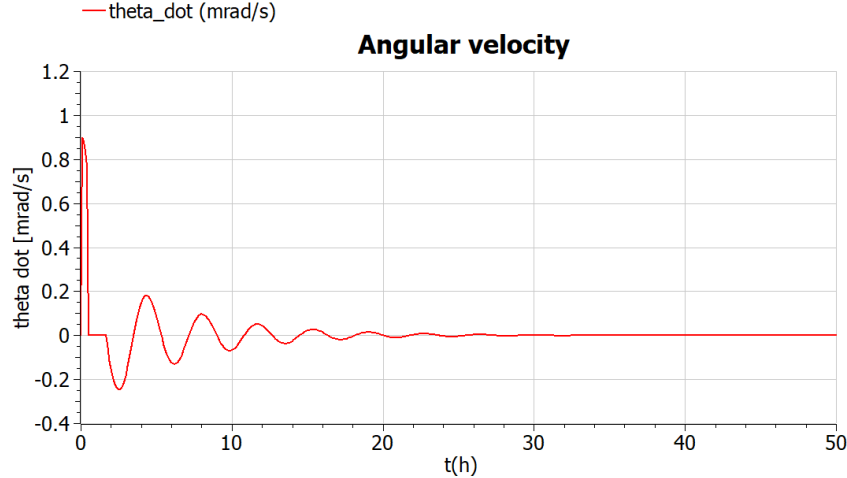
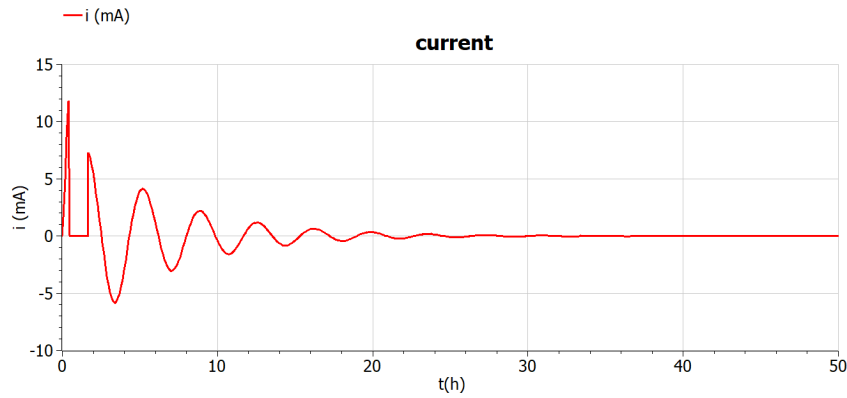


Figure 16: Dymola $\theta(t)$ evolution

**Figure 17:** Dymola $\dot{\theta}(t)$ evolution**Figure 18:** Dymola current evolution

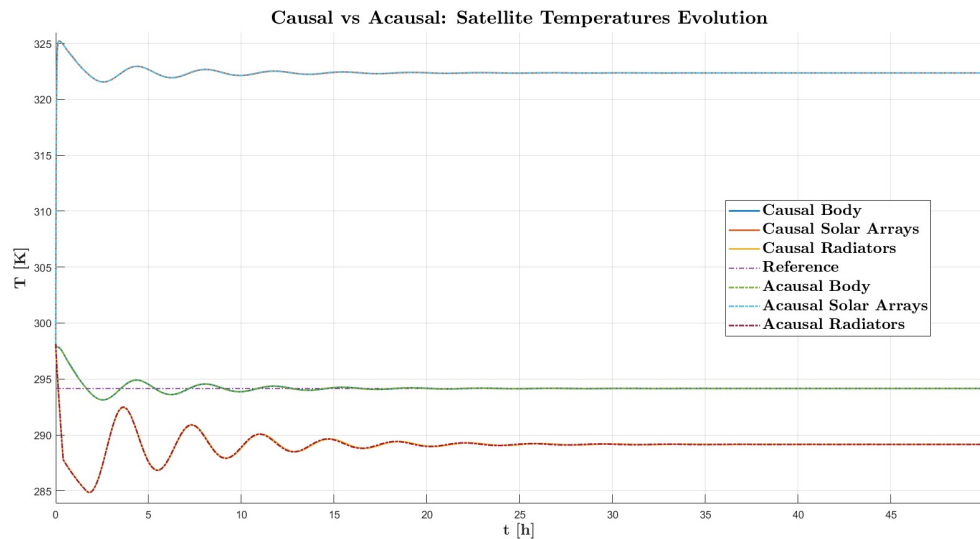
As expected, the results are extremely close to the one of the causal model. As shown in Figure 14, the nodes temperature evolution not only has the same trend of the one showed in Figure 6 but also presents the same behaviour in the proximity of 10 hours as depicted in Figure 15. Analogically, also θ and $\dot{\theta}$ follows the same trend of the causal one. The coincidence for the temperatures and the opening should not be surprising since they both describe the same problem, and also the underlying equations are the same, with the same parameters and control logic. An appreciable difference is related to the current trend, which is considerably different from the one obtained from the causal modeling, as later explained. This is related to a more accurate description of a real DC motor in contrast to the DC motor simple model adopted in the causal model, which does not present any loss. The acausal modeling allows also to launch an animation to better visualise the radiators opening dynamics.

The following table highlights the final nodes temperatures obtained from the acausal model.

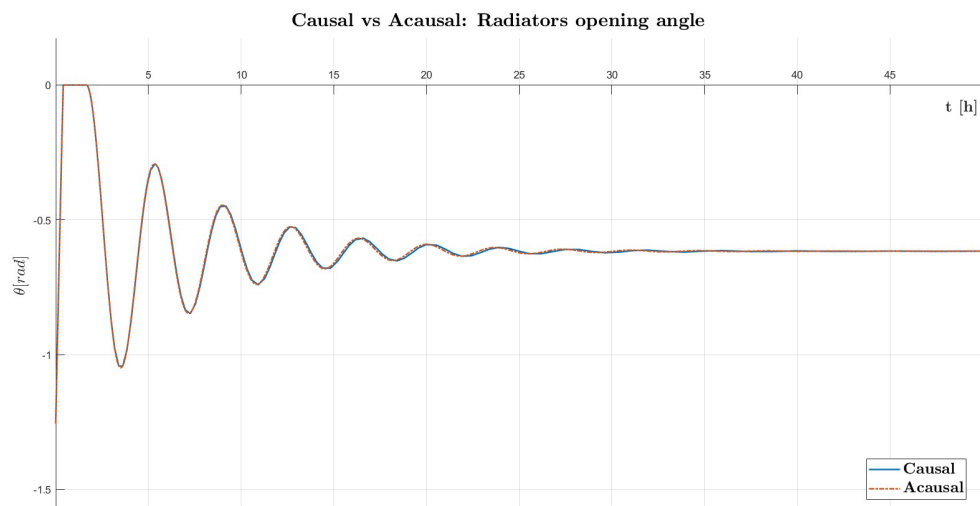
T_{body} [K]	T_{SA} [K]	T_{rad} [K]
294.1497	322.3572	289.1514

Table 8: Dymola: Nodes temperature after 50 hours

The following plots show a comparison between the causal and acausal models, focusing on the notes temperature and on θ :

**Figure 19:** Causal vs Acausal: nodes temperature

A similar trend is shown by the temperature nodes, suggesting a proper modeling of the thermal domain system in Dymola, as expected by steady state simulation runned in Dymola.

**Figure 20:** Causal vs Acausal: radiator opening angle θ

Analysing the angular velocity, it can be noted a difference in the initial transient caused mainly by the DC motor response.

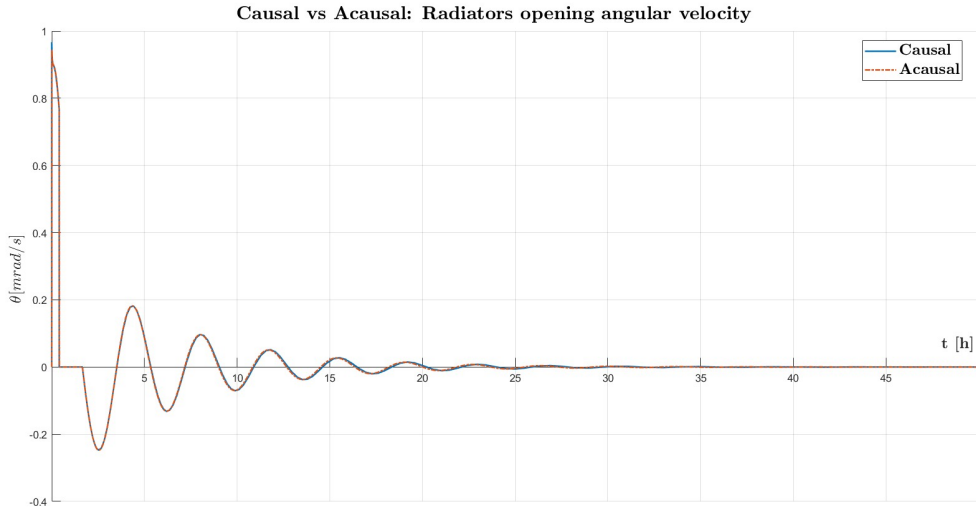


Figure 21: Causal vs Acausal: radiator opening angular velocity $\dot{\theta}$

Following an initial transient phase in which the causal model's current exhibits a larger amplitude, the average value during the subsequent time period is significantly lower than that of the acausal model, as illustrated in Figure 22.

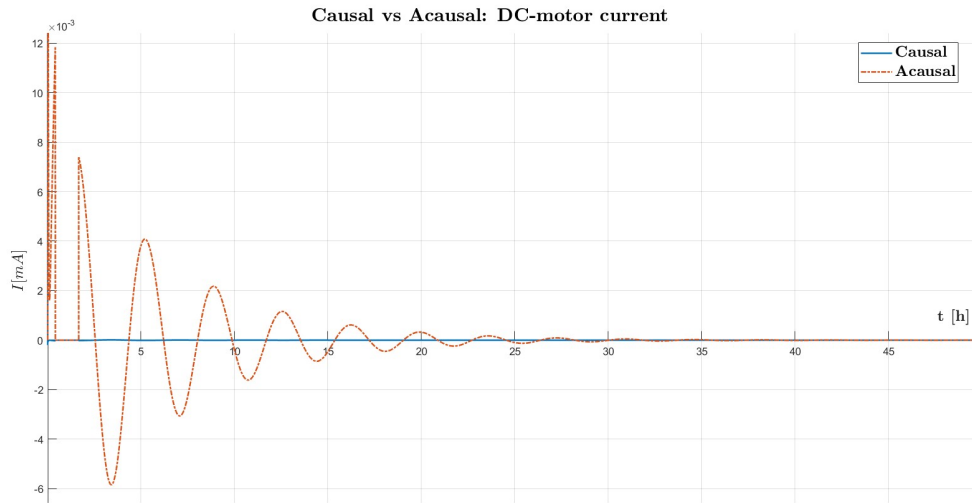


Figure 22: Causal vs Acausal: zoom on DC motor current

The complete current comparison is reported in Figure 53, in Appendix.
Noticeable differences are present in the time evolution of $\dot{\theta}$ and I . The primary discrepancies between the two models are mainly due to:

- **DC Motor Modeling:** The key difference between the two models lies in how the DC motor is represented. In the causal model, it is depicted using an RL circuit and a proportional relationship between current and torque, ignoring any thermal and mechanical losses. Conversely, the acausal model includes undesired losses in the DC motor block, significantly affecting the overall model, leading to major discrepancies in $\dot{\theta}$ and I compared to the causal model. This behavior is observable in a minor part in $\theta(t)$ in Figure 20.



- **Minor Differences in Variables' Time Evolution:** Using two different logical approaches to model the same physical system results in minor differences, primarily influenced by the solver employed. Specifically, *ode23_s* computes the solution at only 253 points, while DASSL does so at 5006 points. To analytically compare the two models without compromising accuracy through methods like interpolation or fixed-step solvers, the integral mean value of the main variables is used to calculate the relative mean error, using the causal model as the reference. The results are presented in Table 13.

Parameter	T_{body}	T_{SA}	T_{rad}	θ	$\dot{\theta}$
Percentual Error	0.000123%	0.000683%	0.000898%	0.0536%	1.0670%

Table 9: Percentual errors between Causal and Acausal integral mean value

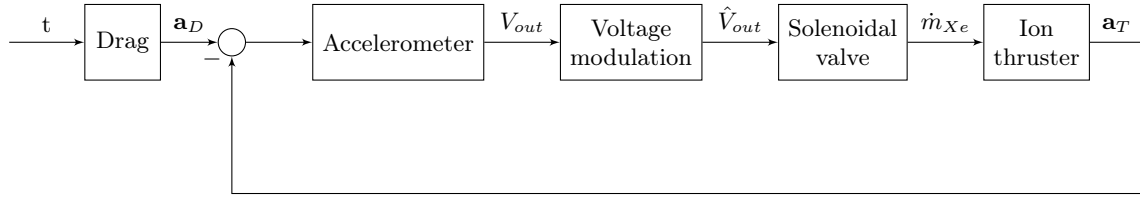
The percentual errors for temperatures are relatively small indicating that the discrepancies between the causal and acausal models for the thermal domain are minimal. However, the error for $\dot{\theta}$ is significantly larger, highlighting a more substantial difference in the time evolution of this parameter between the two models. This larger error states again the impact of DC motor modeling differences, solver variations and particularly in the high parameters sensitivity.

The comparative analysis between causal and acausal modeling approaches reveals distinctive characteristics in their representation of system dynamics. A critical examination of the results highlights two primary areas of divergence. The fundamental distinction lies in the DC motor representation methodology, where the causal approach employs an idealized RL circuit model with a linear current-torque relationship, deliberately omitting thermal and mechanical losses. In contrast, the acausal implementation incorporates these loss mechanisms within the DC motor block, resulting in notable variations in current (I) profile. Indeed, the acausal model shows a current in the order of 10^{-5} mA whereas the causal in the order of 10^{-7} mA . This major difference is related to the modeling of the DC through a Dymola build-in block, which inherently presents power losses (reported in the appendix Figure 49) and so requests an higher current to face these losses.

Despite the acausal approach's advantages in component-based modeling, these findings emphasise the necessity of preliminary causal modeling as a validation tool, especially for complex electromechanical dynamics where model differences are most pronounced. The control could be enhanced using a PID control logic, which takes into account the derivative and the integral of T_1 , consenting to have a smoother and finer radiators rotation.

Exercise 2

A simplified conceptual map of the Attitude Control System (ACS) of a satellite is depicted in Figure 23. For the accuracy of some measurements that the spacecraft has to obtain, the probe has to fly in an orbit very close to the Earth's surface. The spacecraft is therefore subjected to a high atmospheric drag. The ACS has to compensate for the deceleration caused by this drag continuously. In general, ACSs are made of 3 sensors in orthogonal directions and 3 thrusters to detect and compensate for linear and angular accelerations on the probe in each direction, but for the sake of this project, only compensation in the tangential direction will be considered. The ACS is modeled with several modules: an **accelerometer** measuring the accelerations acting on the spacecraft, a **voltage modulation block** controlling the output voltage, the **control valve** modifying the aperture of the thruster valve, and the **ion thruster**.

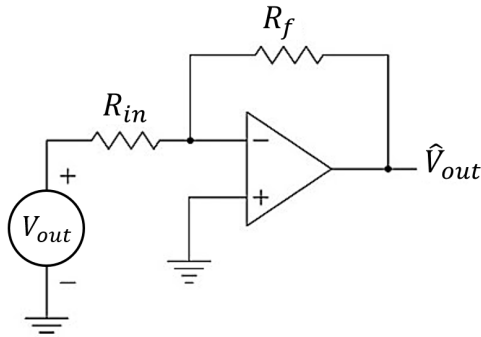
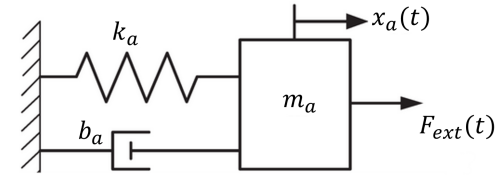
**Figure 23:** Block diagram of the ACS.

The accelerometer, kept aligned with the direction of velocity, presents inside a seismic mass that is subject to an external acceleration \mathbf{a}_D and the thrust T , respectively. The mass is in between the stators of a condenser and, moving for the acceleration given by these two forces changes the output voltage V_{out} of the circuit of the accelerometer. The dynamics of the seismic mass itself can be modeled as a mass-spring-damper system as follows

$$\dot{x}_a = v_a \quad (9)$$

$$F_{ext}(t) = \frac{T - D}{M_{SC}} m_a = m_a \dot{v}_a + b_a v_a + k_a x_a \quad (10)$$

where M_{SC} is the mass of the spacecraft, m_a is the seismic mass value, and b_a and k_a are respectively the damper and the spring terms present in the accelerometer. For the causal modeling, consider the V_{out} as directly proportional to the velocity of the seismic mass, as $V_{out} = K_{acc} v_a$ [1].

**Figure 25:** Inverting operational amplifier.**Figure 24:** Model of the accelerometer.

The output of the accelerometer V_{out} needs to be modulated into \hat{V}_{out} to adjust the control for the solenoidal valve. This modulation is performed through an operational amplifier, displayed in Figure 25. The operational amplifier in inverting configuration modifies V_{out} into \hat{V}_{out} accordingly to:

$$\hat{V}_{out} = -\frac{R_f}{R_{in}} V_{out} \quad (11)$$

where R_f and R_{in} are the two resistances modifying the input voltage.



The voltage \hat{V}_{out} is itself the input of the solenoidal valve, shown in Figure 26, and creates a current I commanding the flow control valve. The current passes through a circuit modeled with only a solenoid with a variable inductance $L(x_v)$. As the current variably flows, a magnetic field is generated. A resulting force f_v acts on the spool, which as a result moves. The armature-spool arrangement is then modeled again as a lumped parameter spring-mass-damper system

$$\dot{x}_v = v_v \quad (12)$$

$$m_v \ddot{v}_v = -k_v x_v - b_v v_v + \frac{1}{2} I^2 \frac{dL}{dx_v} \quad (13)$$

$$\dot{I} = \frac{1}{L(x_v)} \hat{V}_{out} \quad (14)$$

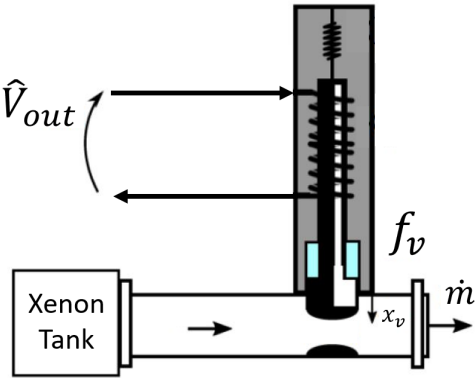


Figure 26: Model of the solenoidal valve.

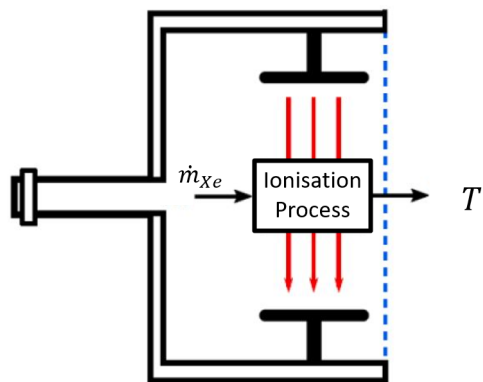
where x_v and v_v represent the position and velocity of the spool, and b_v and k_v are respectively the damper and the spring terms, and m_v is the mass of the spool. The dynamics of the current I is generated by \hat{V}_{out} through the variable inductance $L(x_v) = \frac{1}{\alpha + \beta x_v}$, depending on the position of the valve itself. As the spool moves, the area $A_v(x_v)$ of the duct through which a Xenon flow is passing changes. The resulting mass flow rate \dot{m}_{Xe} of Xenon is ejected into the ion thruster, shown in Figure 27. In particular, the area of the valve can be modeled as

$$A_v(x_v) = A_0 + \ell(x_{v,\max} - x_v) \quad (15)$$

In particular, the orifice area $A_v(x_v)$ has been modeled as linearly varying with x_v . The tool controlling the area is a flap of width ℓ and maximum extension $x_{v,\max} = \ell$, for simplicity.

The value A_0 is the minimum area of the orifice, such that:

$$0 \leq x_v \leq x_{v,\max}$$



$$A_0 = \underbrace{A_v(x_{v,\max})}_{\text{minimum area}} \leq A_v \leq \underbrace{A_v(0)}_{\text{maximum area}} = A_0 + \ell^2 \quad (16)$$

The ion thruster comprises an ionization chamber that utilizes a strong magnetic field, ionizing the Xenon flux. The generated ions are moved towards the acceleration grid, which accelerates the ions using a strong electric field, producing a thrust on the spacecraft as the final effect. The flux of Xenon \dot{m}_{Xe} can be expressed as follows

$$\dot{m}_{Xe} = A_v(x_v) \sqrt{k \rho_{Xe} p_T \left(\frac{2}{k+1}\right)^{\frac{k+1}{k-1}}} \quad (17)$$

where $\rho_{Xe} = \frac{p_T}{\bar{R}T_T}$, k and \bar{R} being respectively Xenon specific heat ratio and gas constant. In the tank, the gas is at a total pressure of p_T and temperature of T_T . The Xenon flow enters the thruster and is here ionized into ions with mass m_i and charge q . After the acceleration imposed



by the acceleration grid with a voltage ΔV , the ions exit from the nozzle with a velocity v_{exit} , producing the thrust T , as follows

$$T = \dot{m}_{Xe} v_{exit} = \dot{m}_{Xe} \sqrt{\frac{2q\Delta V}{m_i}} \quad (18)$$

Table 10 reports the values for the parameters to simulate the ACS system, with symbol and unit of measure. The drag $D(t)$ can be modeled as a function of time only, as it follows

$$D(t) = 2.2 - \cos(\omega_s t) + 1.2 \sin(\omega_o t) \cos(\omega_o t) \quad (19)$$

where t enters in seconds, and $D(t)$ is in mN.

Component	Parameter	Symbol	Value	Unit
Accelerometer	Spacecraft mass	M_{SC}	300	kg
	Seismic mass	m_a	0.32	kg
	Accelerometer damper	b_a	[$1.5 \cdot 10^3$ – $2 \cdot 10^4$]	Ns/m
	Accelerometer spring	k_a	[$5 \cdot 10^{-5}$ – $3 \cdot 10^{-3}$]	N/m
	Acc. proportional coefficient	K_{acc}	1	Vs/m
Amplifier	Inverting resistance	R_{in}	[0.1–10]	Ω
	Feedback resistance	R_f	[$1 \cdot 10^4$ – $8 \cdot 10^4$]	Ω
Solenoidal Valve	Spool mass	m_v	0.1	kg
	Valve spring	k_v	$1 \cdot 10^3$	N/m
	Valve damper	b_v	$1 \cdot 10^3$	Ns/m
	Solenoid constant	α	$2.1 \cdot 10^{-2}$	1/H
	Solenoid gain	β	-60	1/Hm
	Minimum area	A_0	$4.7 \cdot 10^{-12}$	m^2
	Maximum extension	$x_{v,\max}$	$1 \cdot 10^{-5}$	m
Thruster	Heat ratio	k	1.66	-
	Tank pressure	p_T	$2 \cdot 10^5$	Pa
	Tank temperature	T_T	240	K
	Gas constant	\bar{R}	63.32754	J/kg K
	Charge	q	$1.6 \cdot 10^{-19}$	C
Drag	Voltage	ΔV	2000	V
	Ion mass	m_i	$2.188 \cdot 10^{-25}$	kg
	Secular pulsation	ω_s	$1.658226 \cdot 10^{-6}$	rad/s
	Orbital pulsation	ω_o	$1.160758 \cdot 10^{-3}$	rad/s

Table 10: Parameters for the simulation of the ACS.

Part 1: causal modeling (9 points)

Reproduce in Matlab the physical model of the ACS, in particular

1. Formulate the full system of non-linear ODEs making explicit the state variables of the whole simulation. Tune the values of the parameters not explicitly stated in Table 10 to have the compensating thrust T the most similar to the disturbing drag D .
2. Choose the appropriate initial conditions and simulate for three orbital periods T_o , where $T_o = 2\pi/\omega_o$.
3. Discuss the selection of the ODE integration scheme.

(9 points)



- The model has the role to reproduce an Attitude Control System (ACS), which compensates the atmospheric drag caused by the probe's orbit, thanks to an ion thruster. Through a series of signals, the derived acceleration read by the accelerometer is able to provide a thrust capable of compensating the drag. There is an intrinsic limit caused by the system response, which introduces a mismatch between the drag and thrust and, therefore, a small non-null force acting on the probe. The physical model of the ACS is composed of a set of electrical and mechanical modules, listed below:

- Accelerometer*, modeled through a lumped parameter mass-spring-damper model has the role to measure the difference between drag and thrust and give as output a signal voltage directly proportional to the seismic mass. Its dynamics is described through the state variables $[x_a \ v_a]$, obtained through the resolution of a second-order differential equation, written as a system of linear ODEs:

$$\begin{cases} \dot{x}_a = v_a \\ \dot{v}_a = \frac{T - D}{M_{sc}} - \frac{b_a}{m_a} v_a - \frac{k_a}{m_a} x_a \end{cases} \quad (20)$$

- Voltage Modulator*, modeled through an inverting operational amplifier, modulates the accelerometer output voltage V_{out} into \hat{V}_{out} , to properly drive the solenoidal valve.
- Solenoidal Valve*, is the most complex element of the system and its behaviour totally influences the capability of the ACS to properly damp the external drag. The solenoidal valve creates a current I and, through a variable inductance L , generates a Lorenz force f_v that drives an armature-spool, modifying the Xenon orifice area. The armature-spool system is modeled through a lumped parameter mass-spring-damper system. The solenoidal valve is described by the state variables $[x_v \ v_v \ I]$, obtained through the resolution of the following system of linear ODEs:

$$\begin{cases} \dot{x}_v = v_v \\ \dot{v}_v = -\frac{k_v}{m_v} x_v - \frac{b_v}{m_v} v_v + \frac{1}{2 m_v} I^2 \frac{dL}{dx_v} \\ \dot{I} = \frac{\hat{V}_{out}}{L} \end{cases} \quad (21)$$

It is important to highlight that the variable inductance L is modeled as depending on the position of the valve itself. In addition, the valve stroke should not exceed its physical constraints, limiting its behaviour to the limit case in situations where the ACS would require an higher thrust than the one suppliable by the solenoidal valve and ion thruster system.

- Ion Thruster*, is the element that physically generates the thrust by the acceleration of the Xenon ions via electro-magnetic forces. Its behaviour is simplified without considering any losses, depending only on the Xenon mass flow rate, which is a function of the orifice area A_v .

The atmospheric drag is a function of time only and is not influenced neither by the probe's attitude nor by the thrust module, allowing to decouple and simplify the problem.

The ACS behaviour strongly depends on the accelerometer and voltage modulator parameters, which has to be selected in order to optimise the attitude control system compensation, trying to follow as fast and precisely as possible the drag time evolution. The optimisation logic is based on the minimisation of the cost function $J = \frac{1}{n} \sum_{i=1}^n (T_i - D_i)^2$, where n represents the time steps. Parameter optimization is carried out through iterative



research based on the *genetic algorithm*, whose peculiarity allows the parameter domain region to be efficiently scanned.

Parameters	b_a [Ns/m]	k_a [N/m]	R_f [Ω]	R_{in} [Ω]
Value	$1.51041 \cdot 10^3$	$4.39645 \cdot 10^{-4}$	0.1078	$7.7306 \cdot 10^4$

Table 11: Accelerometer and Voltage modulator optimal parameters

It is worth mentioning that the optimal parameters are close to the boundary values. The accelerometer mass-spring-damper is a highly overdamped system ($\zeta = 63670$), which allows the system not to introduce spurious and dangerous oscillations. Furthermore, the real parameter to optimise for the voltage modulator is the feedback resistance ratio.

2. To properly simulate the ACS response is necessary to properly define initial conditions.

- *Null initial state conditions*, which mimic the commissioning of the ACS. It starts with maximum initial error, $A_v = A_{v,max}$, and subsequently rapidly converges and follows the drag evolution.

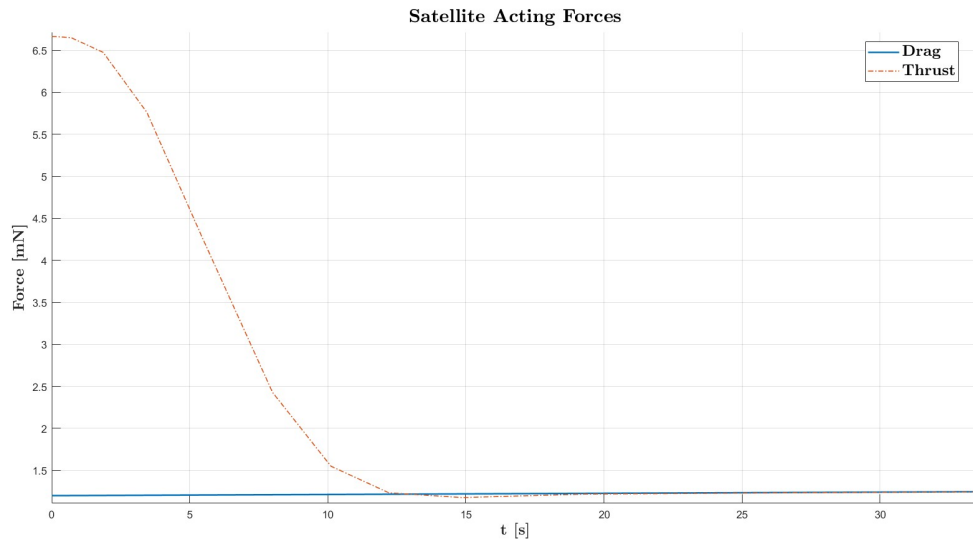


Figure 28: Zoom on thrust drag time evolution with null initial state conditions

- *Initial null error*, allows to start with a thrust that fully compensates the drag.

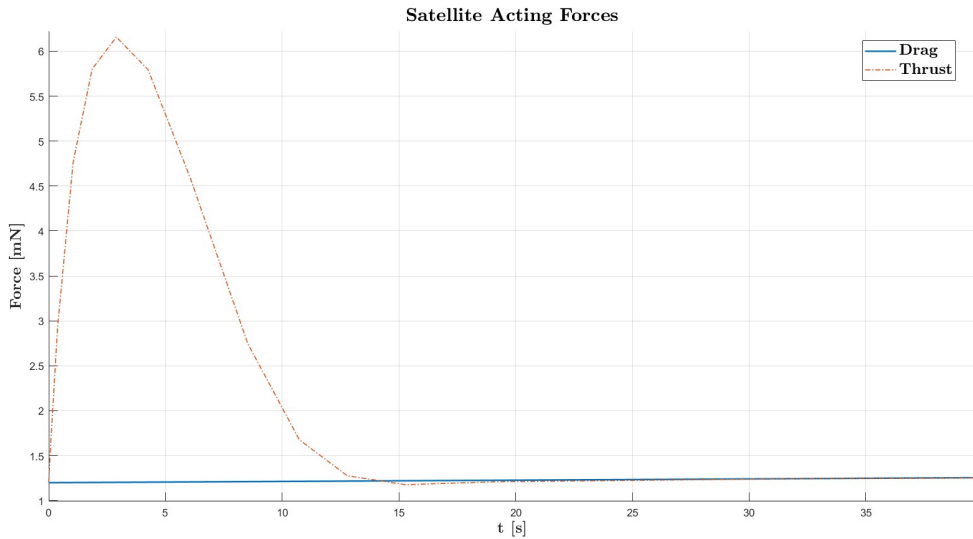


Figure 29: Zoom on thrust drag time evolution with initial null error

Regardless the initial null error, the system overshoots the initial thrust trend due to the internal system response and time costant, which consents to properly follow the drag evolution only after 15 s. The null initial state conditions, instead, start with the initial maximum error but allows to rapidly and more linearly follow the drag behaviour, showing the ACS system response and initial calibration; furthermore, this initial condition best simulates a real mission scenario, where the ACS commissioning takes place. Indeed the percentual relative error ($e_{rel,\%} = 1.4291\%$) is lower with null initial conditions than with null initial error ($e_{rel,\%} = 1.5235\%$).

According to this rationale, the simulation is carried out using initial null conditions.

Carrying the simulation for 3 orbits, the following results are obtained:

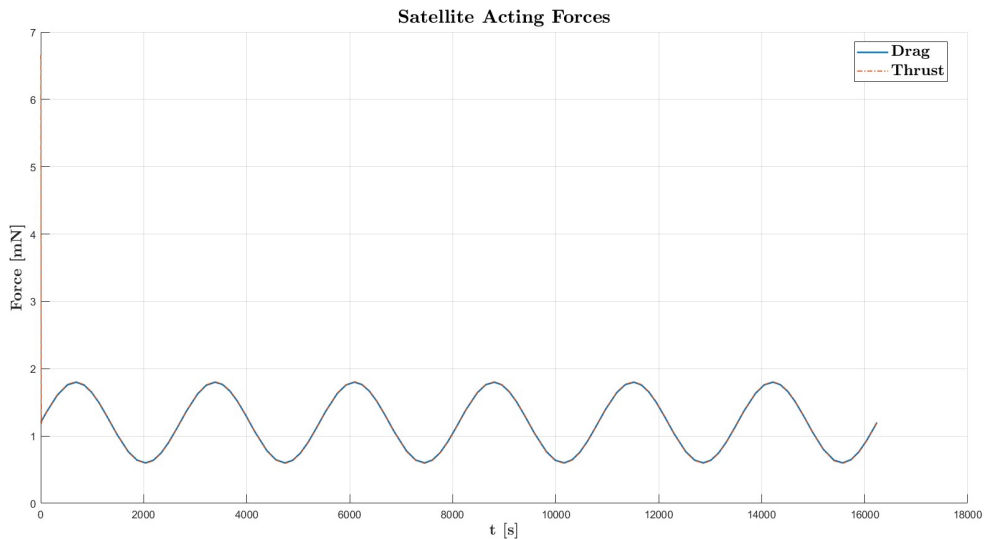
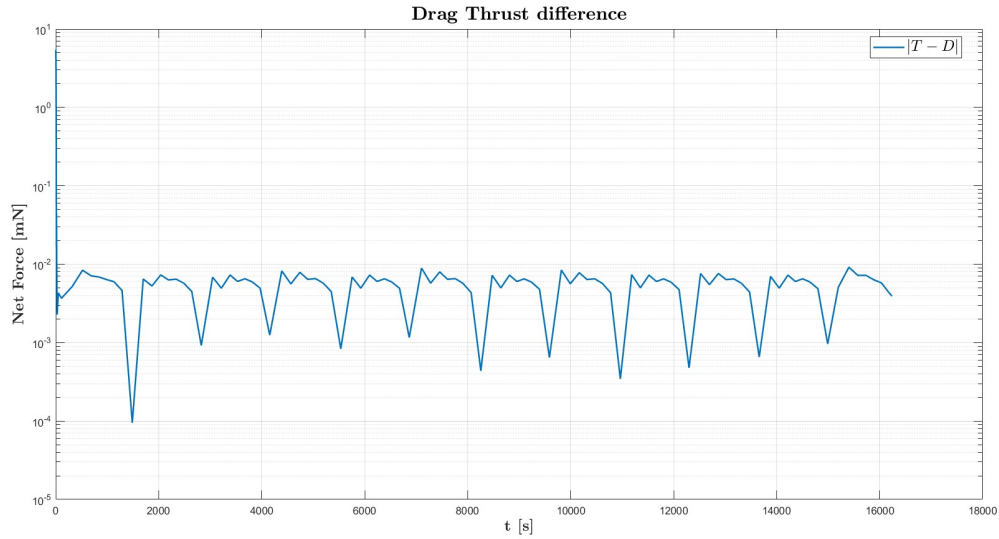
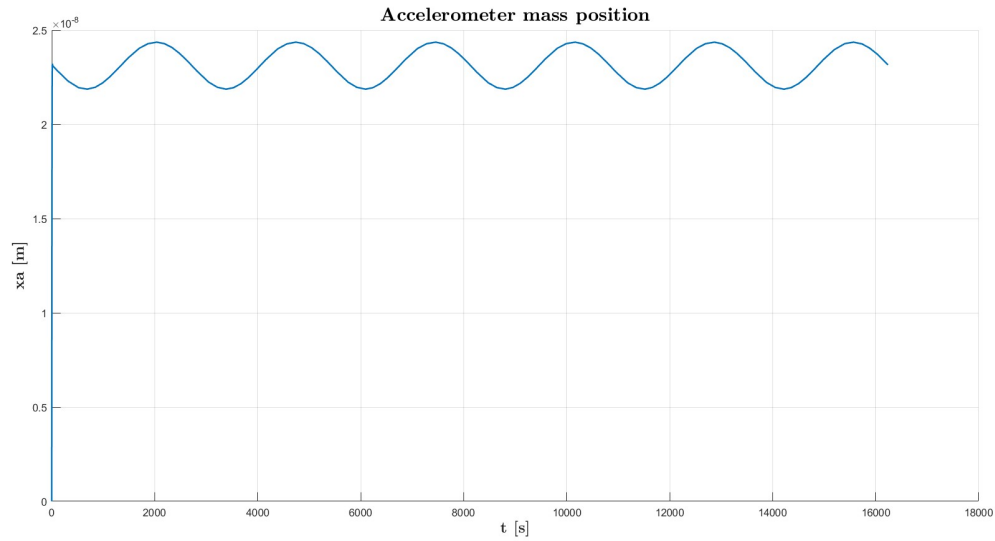


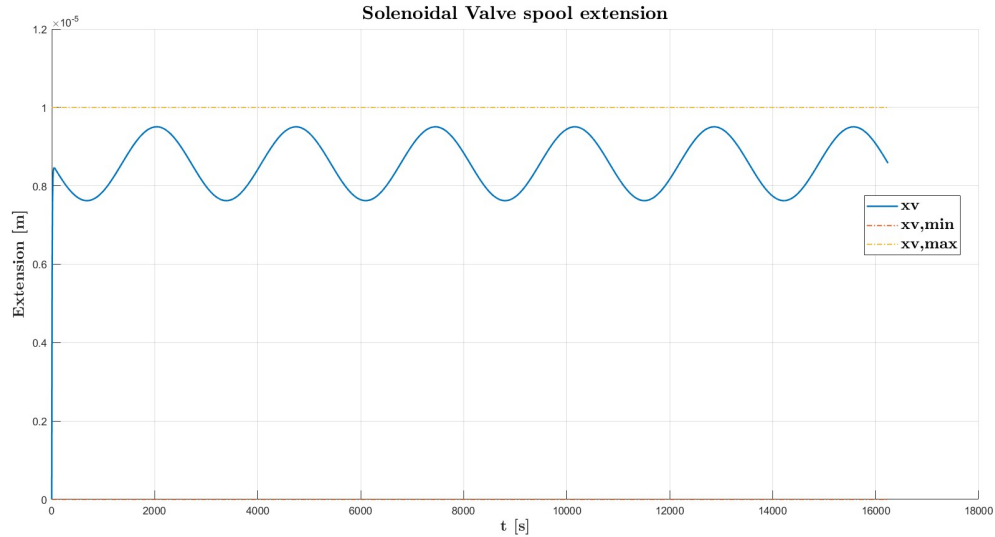
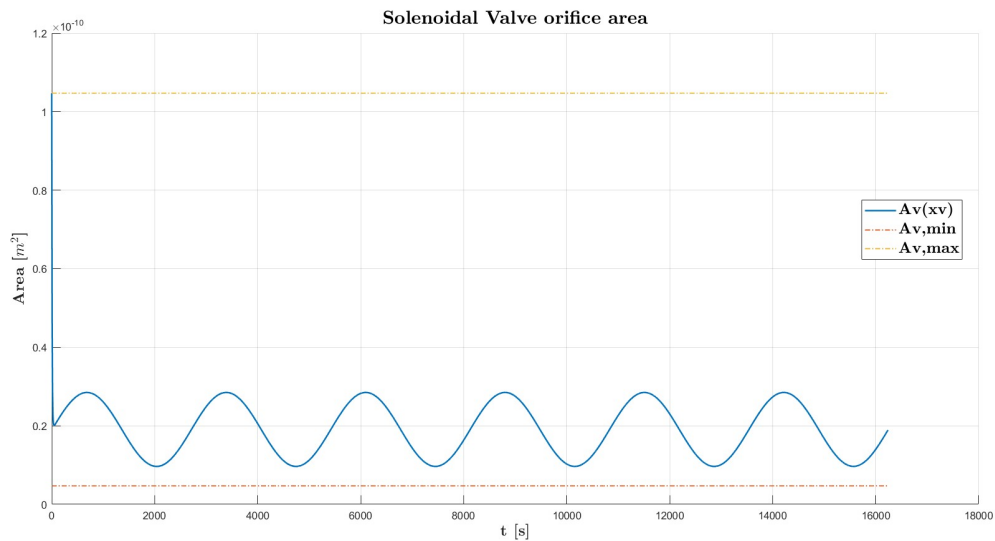
Figure 30: Thrust and Drag time evolution

**Figure 31:** Thrust absolute error

As previously stated, the thrust closely matches and follows the drag evolution after an initial transient dictated by the initial conditions. The mean net force acting on the probe is $3.7832 \times 10^{-4} \mu\text{N}$, which in terms of orbital perturbation and attitude disturbance is not negligible and needs to be properly addressed in order to prevent undesired evolutions. It is also possible to appreciate that the thrust has a sinusoidal shape, resembling drag's sinusoidal time dependence.

**Figure 32:** Accelerometer mass position

The accelerometer shows a sinusoidal oscillation of the seismic mass, which reflects the drag evolution; in addition, the chosen parameters are in the correct range to avoid introducing undesired and spurious acceleration caused by close proximity to the resonance frequency range.

**Figure 33:** Solenoidal Valve spool extension**Figure 34:** Solenoidal Valve orifice area

Analysing the solenoidal valve state variables time evolution, it is possible to spot that the initial condition is related to the maximum orifice area and therefore to the maximum thrust available. With the chosen accelerometer and voltage modulator parameters and initial conditions, the spool extension does not ever exceed its limits, not requiring any logical limiting scheme, expressing a correct behaviour of the ACS and a proper selection of the instruments for the problem in analysis.

3. For simulating the ACS evolution involving a multi-physical domain, ode23s presents distinct advantages over alternative integration methods such as ode45 or ode15s. Ode23s emerges as the optimal choice by effectively balancing computational efficiency and numerical stability for stiff problems. Its adaptive step size is particularly well-suited for handling the different time scales and nonlinear behaviours inherent in the analysed problem. The simulation is carried out with a relative and absolute tolerance of 10^{-11} and the adopted integration scheme computes the solution in 112 time steps.



Part 2: acausal modeling (6 points)

Reproduce in Simscape the physical model of the ACS. Choose the appropriate initial conditions and parameters, simulate for three orbital periods T_o , and compare the results with those obtained in the prior point.

Note: when modeling the solenoid valve in Simscape, please consider the nominal values shown in Table 12.

Parameter	Value	Unit
Pull-in forces $[F_1 - F_2]$	$[9000 - 12]$	N
Stroke $[x_1 - x_2]$	$[0 - 0.1]$	mm
Maximum Stroke	0.1	mm
Rated voltage	0.6	mV
Rated current	0.1	A
Contact stiffness	0.12×10^6	N/m
Contact damping	10^4	Ns/m

Table 12: Solenoid parameters in Simscape.

(6 points)

The acausal model of the system is realised on Simscape. It is more evident from Figure 35 the multi-physical nature of the problem since every module is distinguished by specific domain elements, which, however, are connected in order to get a closed-loop system, typical of attitude control systems.

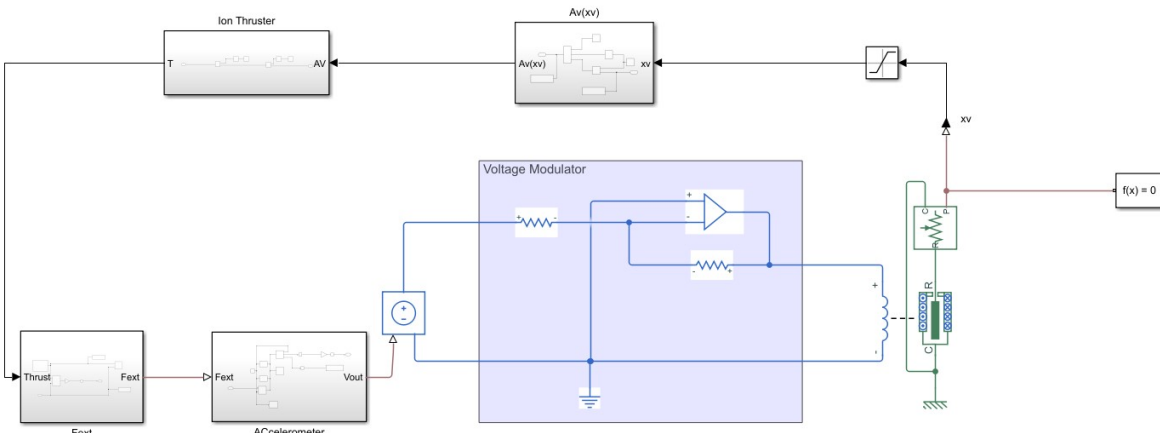


Figure 35: Acausal model of ACS system in Simscape

In particular, the following subsystems are noteworthy:

- *Accelerometer:*

The acausal modeling allows to simply realise the accelerometer model by positioning the mass-spring-damper blocks. The accelerometer output potential is obtained from the product between the seismic mass velocity and the accelerometer proportional constant. Fundamental is to make sure that all the blocks have the same mechanical reference in order to consistently model the system.

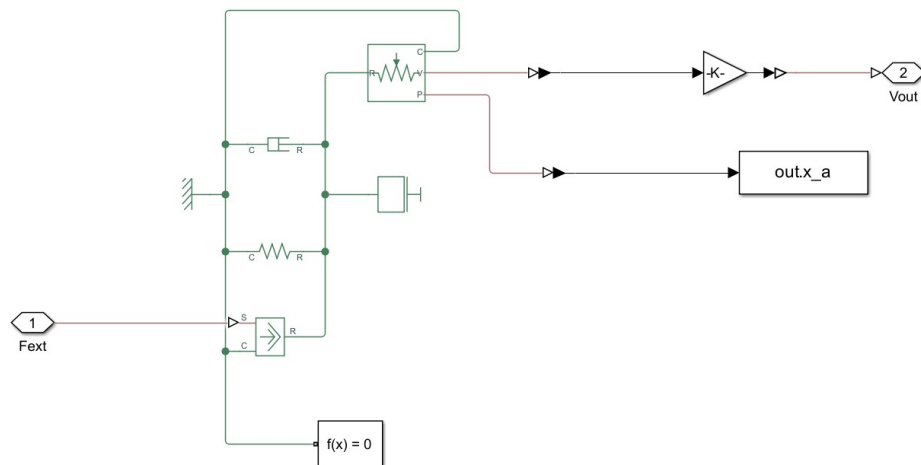


Figure 36: Acausal model of Accelerometer in Simscape

- *Voltage Modulator:*

From Figure 37, it is noticeable that an inverting operational amplifier configuration is realised, posing particular attention on the resistor pole orientation in order to properly invert and scale the input voltage signal into a signal suitable for the solenoidal valve.

- *Solenoidal Valve*

The most important block of the model is the "solenoid" one since it consents with extreme simplicity to model the functioning of the solenoidal valve; however, it is particularly sensitive to its settings. The parameters chosen are reported in Table 12.

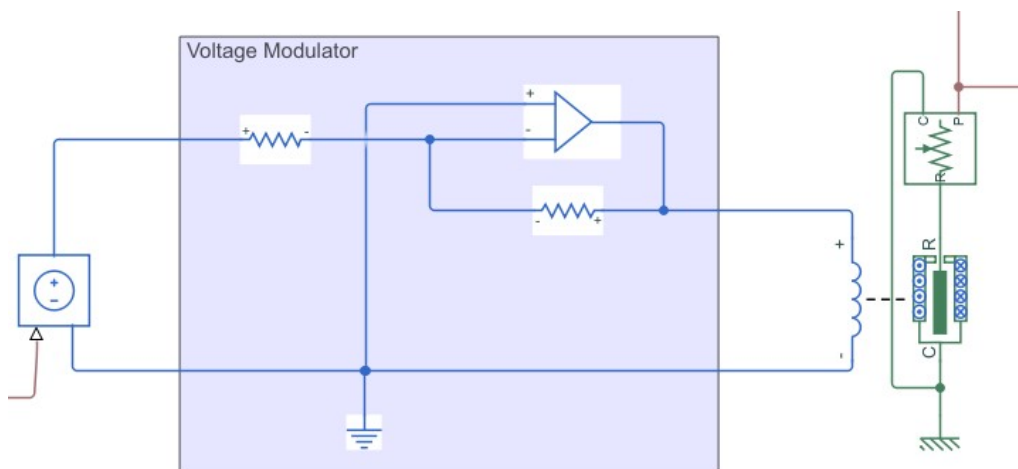


Figure 37: Acausal model of Voltage modulator and Solenoidal valve in Simscape

To limit properly limit the armature spool extension is necessary to place a saturation block since some criticalities are shown by the "solenoid" block on simulating the initial transient.

The simulation is run with a relative and absolute tolerance of 10^{-11} adopting the variable step *daessc*, an implicit solver designed for efficiently handling Differential Algebraic Equations (DAEs), which excels in simulating stiff systems and models with constraints, adjusting time steps dynamically for accuracy and efficiency.

The results are shown in the following plots. As expected, the ACS acausal model is able to properly simulate the problem and provide a thrust that rapidly compensates the drag, showing

a similar time evolution as causal one.

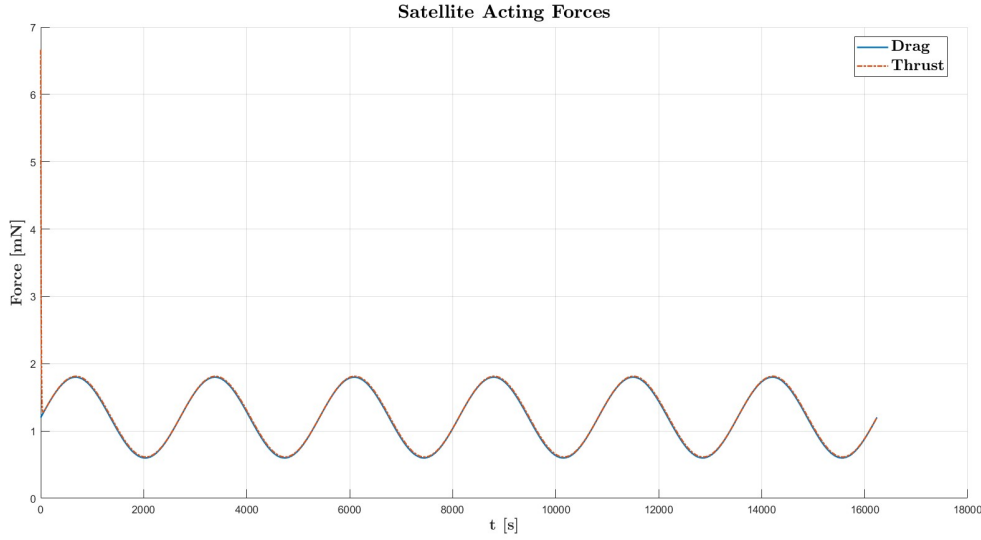


Figure 38: Acausal Thrust Drag evolution

From the logarithmic absolute error between thrust and drag, with respect to the causal reported in Figure 31, it is possible to spot that the error is one order of magnitude higher, suggesting the presence of a criticality in the simulation. The mean net force acting on the probe is $1.495 \cdot 10^{-3} \mu\text{N}$, one order of magnitude higher than the causal one. The trend is smoother than causal's one, indicating the higher computational performance of *daessc* with respect to *ode23s*.

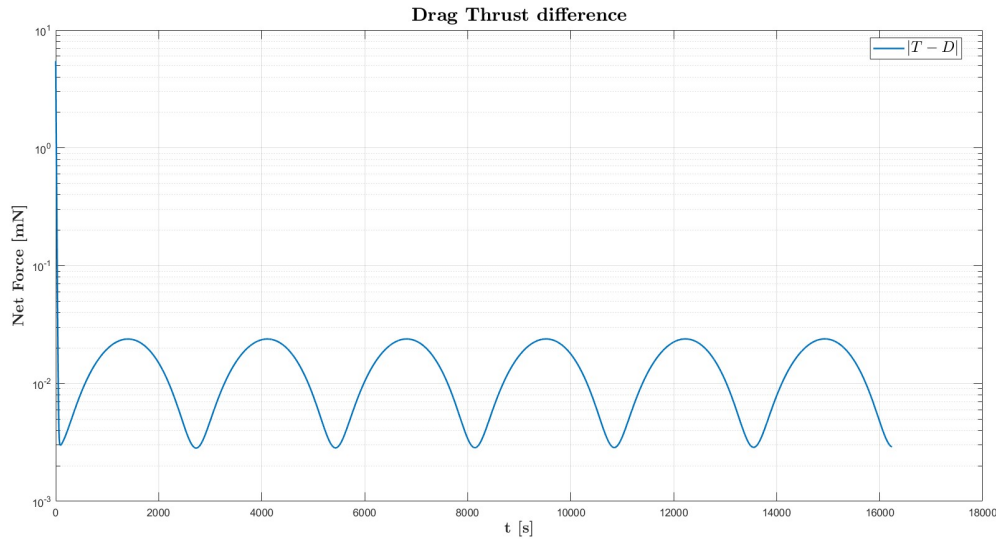
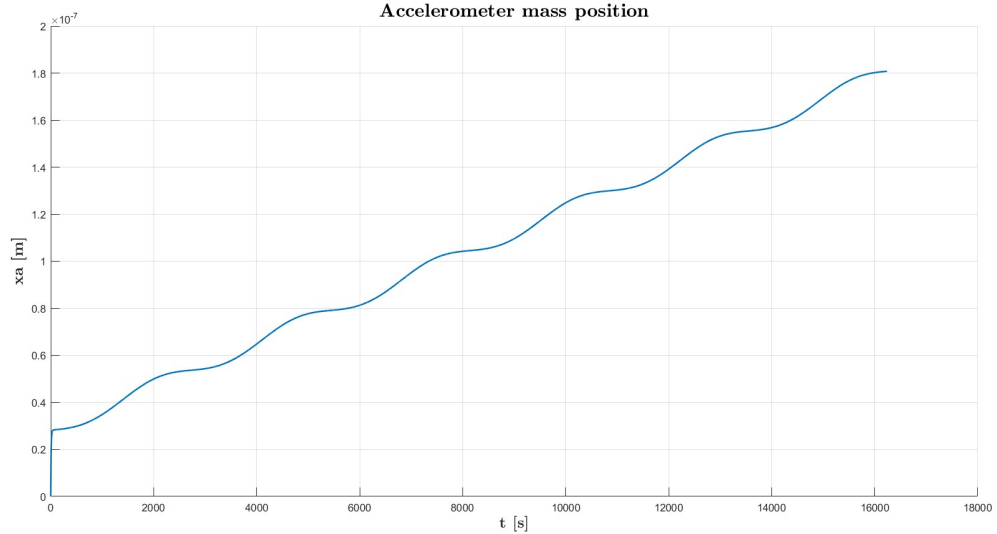
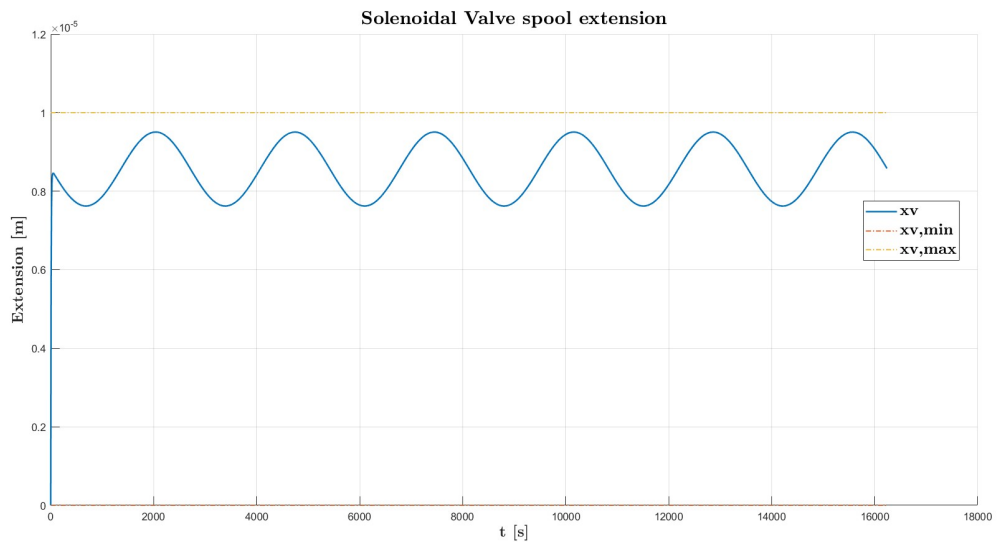


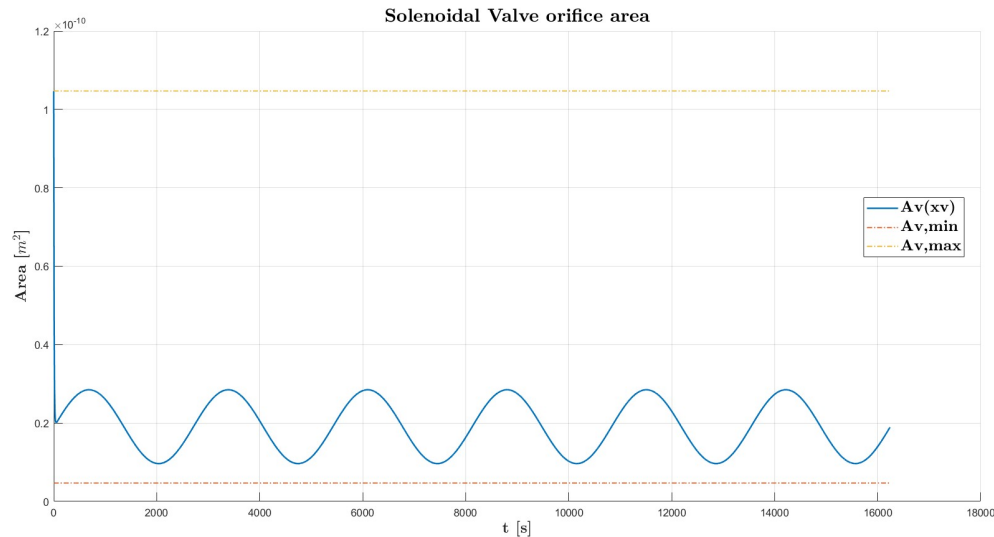
Figure 39: Acausal logarithmic Thrust Drag difference evolution

The accelerometer trend in Figure 40 is completely different from the one obtained in the causal model (Figure 32), observing the composition of a sinusoidal wave and a linear trend. This difference might be attributable to the "solenoid" block, which models the solenoidal valve, being the only ACS element modeled using a proper build-in block rather than composing other blocks to model it.

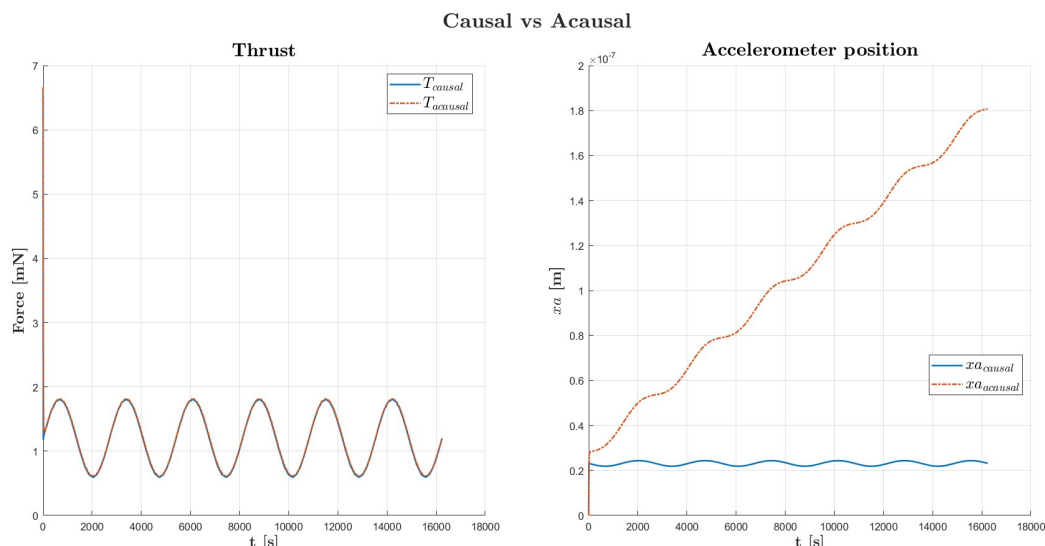
**Figure 40:** Acausal Accelerometer position evolution

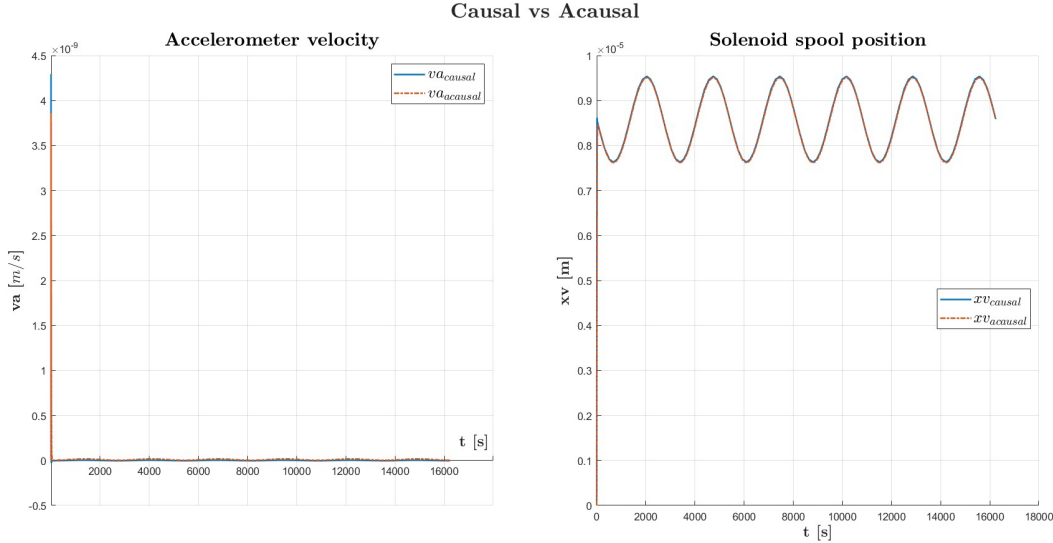
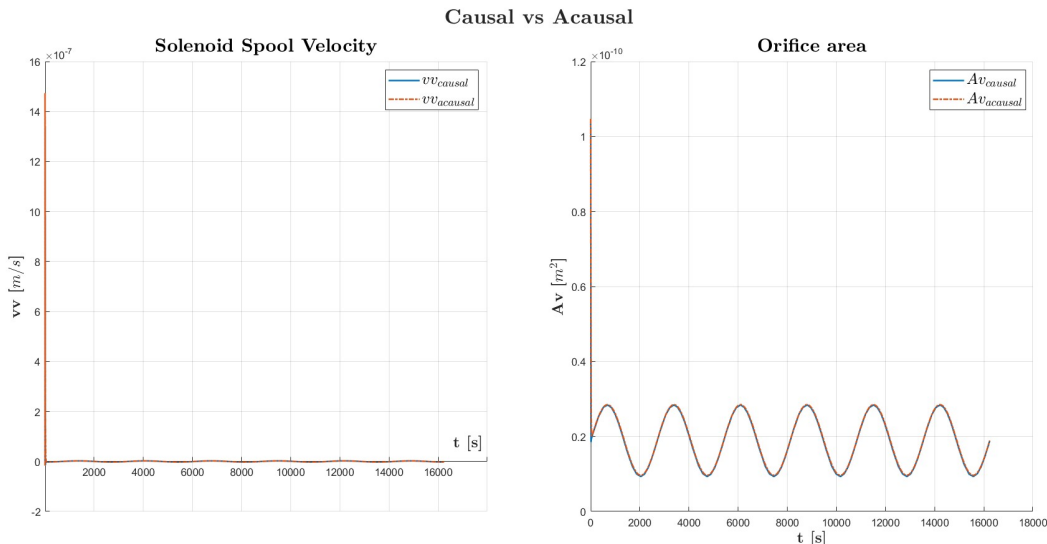
The solenoidal valve extension and orifice area show a similar trend to the causal one, thanks to the introduction of the "saturation" block, which properly handles the initial transient, where a negative overshoot of the solenoidal valve position is observed, reaching negative values. The overshooting behaviour is shown in the Appendix in Figure 54. The saturation block acts only during the initial transient, showing a critical behaviour of the "solenoid" block simulating the first time steps; however, once the ACS starts to properly compensate the drag, the solenoid works appropriately, as observable by the x_v , A_v sinusoidal trend, similar to the causal one.

**Figure 41:** Acausal Spool extension evolution

**Figure 42:** Acausal Valve area evolution

The focus of this simulation is the comparison of the results between the causal and the acausal models. The following figures show the main differences:

**Figure 43:** Comparison between Thrust and x_a

**Figure 44:** Comparison between v_a and x_v **Figure 45:** Comparison between v_v and A_v

The main discrepancies between the two models are mainly related to:

- **Accelerometer seismic mass position x_a**

The employment of the solenoid block introduces undesired behaviors connected to its high parameter sensitivity and high model complexity, regardless of the simplification that introduces for the overall acausal model composition. The substitution of this block with a causal-like logic consents to remove this error and obtain an evolution similar to the causal model. It is useful to highlight that the solenoid constant drift does not affect directly the other variables since the accelerometer output is the voltage, which is strictly dependent on v_a only; indeed, the two models show a similar velocity oscillation frequency, as better appreciable in Figure 56, reported in the Appendix.

- **Minor differences on variables time evolution**

The adoption of two different logical solutions to model the same physical model naturally



leads to minor differences that are mainly dependent on the solver used. In particular, $ode23_s$ computes the solution in only 112 points, whereas daessc in 69674. To analytically compare the two models without using methods which would reduce the solutions' accuracy, such as interpolations or fixed step solvers, the integral mean value of the main variables is used to compute the relative mean error, using the causal model as a reference case. The results are reported in Table 13.

Parameter	x_a	v_a	T	x_v	v_v	A_v	D
Percentual Error	350.67%	678.26%	1.15%	0.25%	0.28%	1.15%	0.01%

Table 13: Percentual errors between Causal and Acausal integral mean values

The difference between solvers is highlighted by the drag percentual error, which in both models is computed through the given time relation. As expected, huge errors are associated with the accelerometer state variables, caused by the accelerometer position constant drift; whereas the solenoid state variables present a lower error, thanks to the introduction of a saturation block for both position and velocity to better handle the initial transient. The acausal model presents indeed a critical handling of the initial transient, which influences the overall simulation along with the demanding choice of the block parameters, in order to properly match the given physical model. The acausal model simplifies the model analysis thanks to the intuitive system composition and better optimised solvers; however, a proper knowledge of the underlying physics is fundamental, also through a preliminary causal simulation, useful to validate the following acausal model.

1 Appendix

1.1 Exercise 1

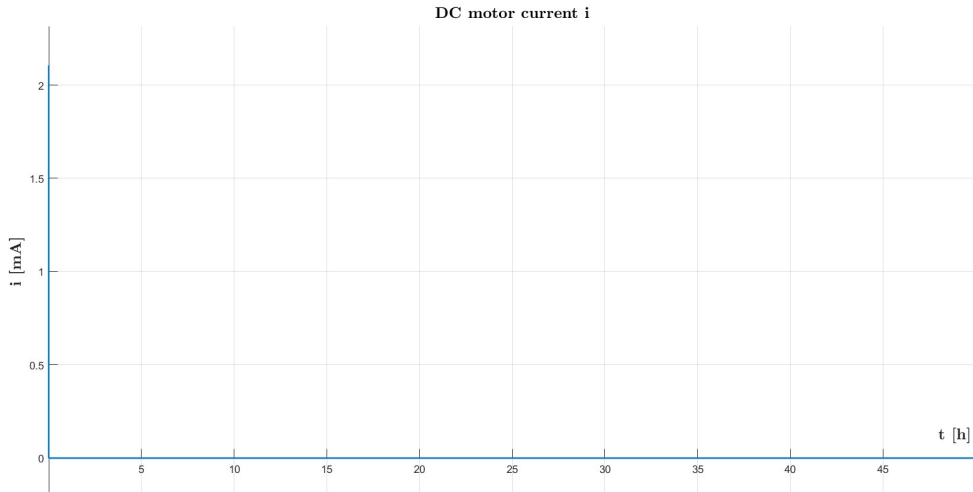
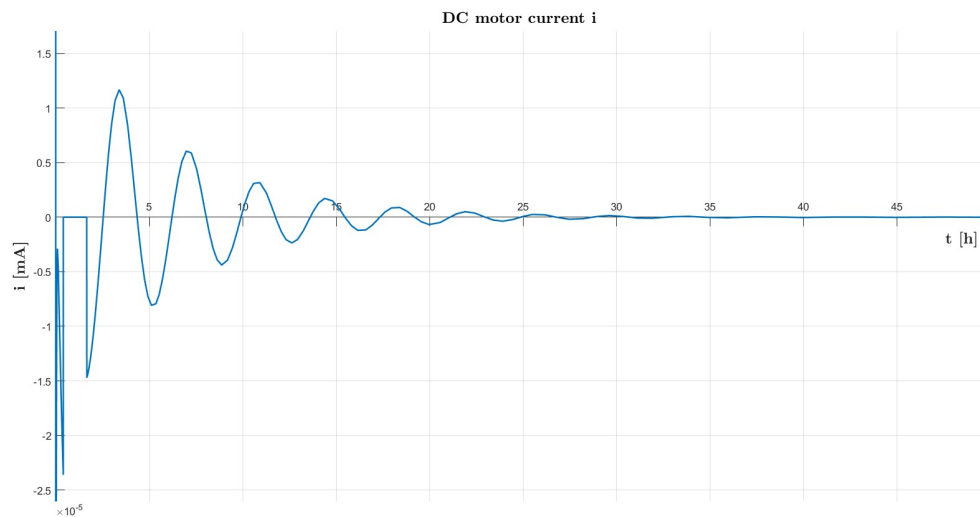
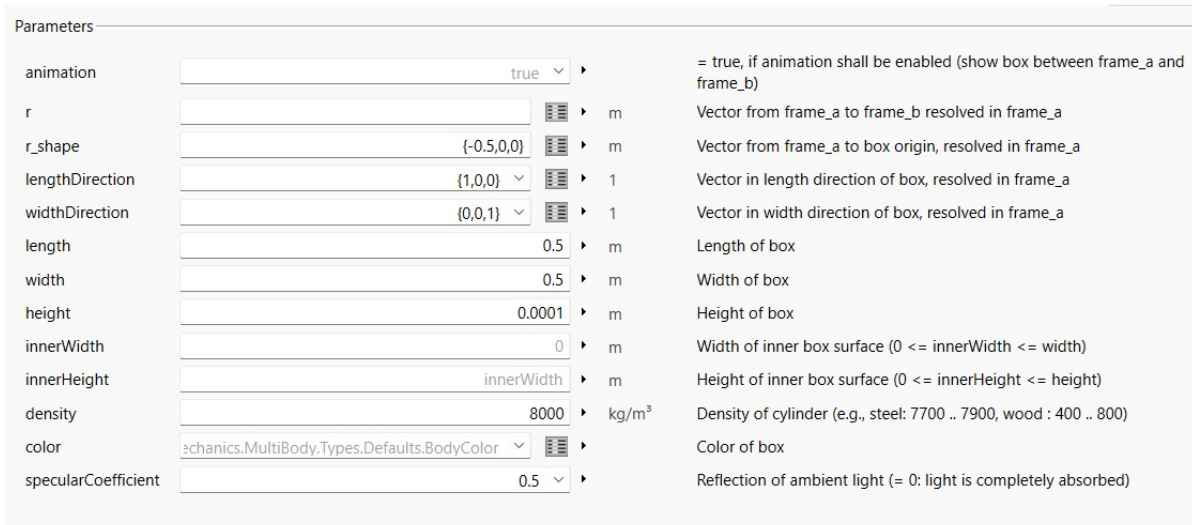


Figure 46: Causal current initial transient

**Figure 47:** Causal current evolution, neglecting initial transient**Figure 48:** Dymola Body Box parameters

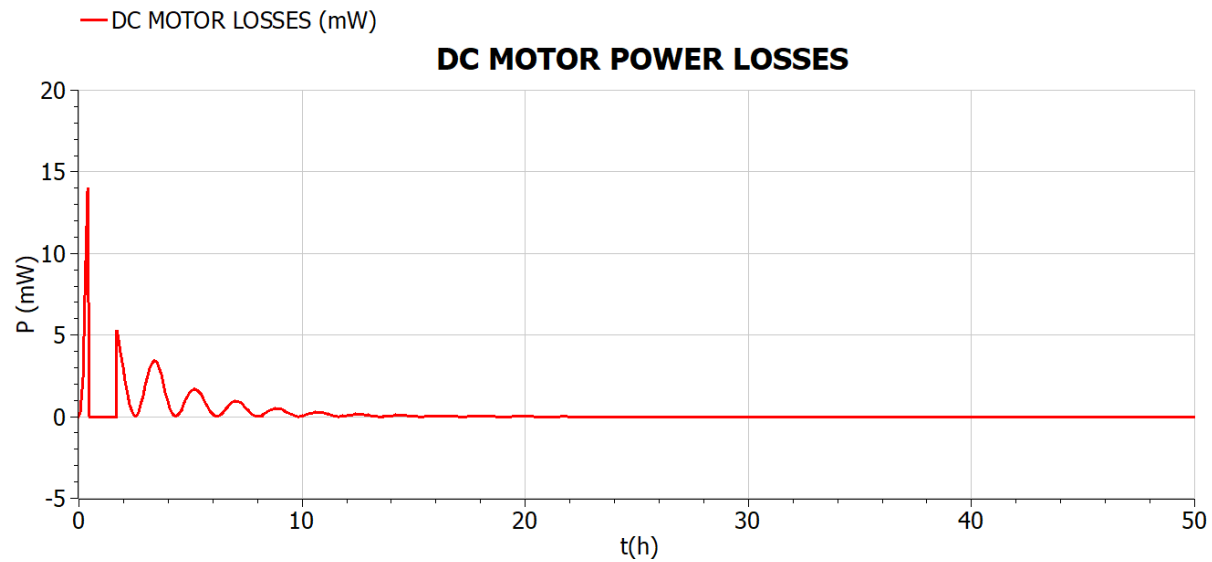


Figure 49: Dymola DC motor losses

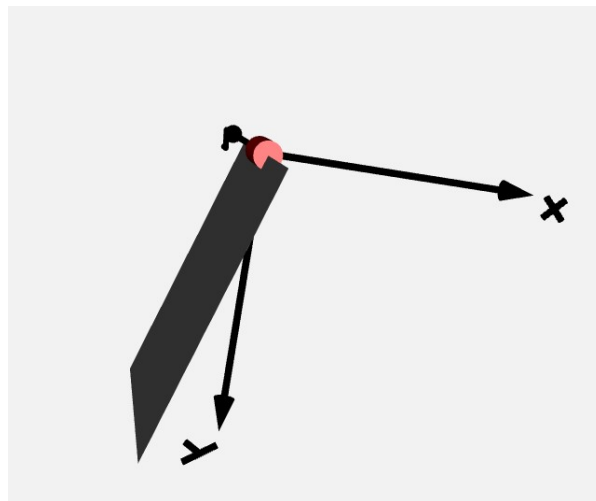


Figure 50: Dymola radiator animation for $\theta(0) = -0.4 \pi \text{ rad}$

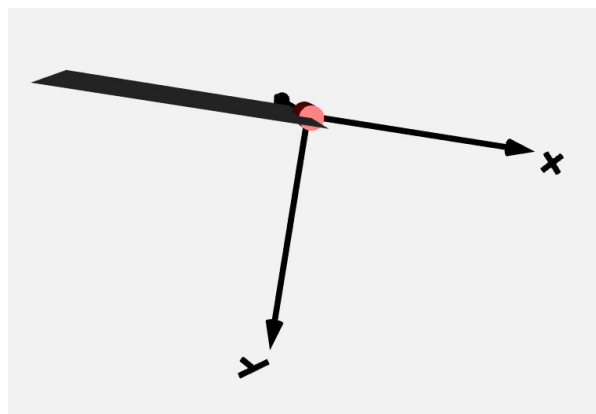


Figure 51: Dymola radiator animation for $\theta_{max} = 0 \text{ rad}$

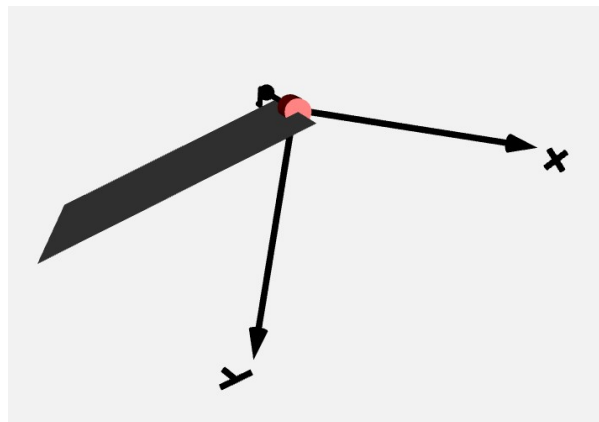


Figure 52: Dymola radiator animation for $\theta_{final} = -0.1962 \pi \text{ rad}$

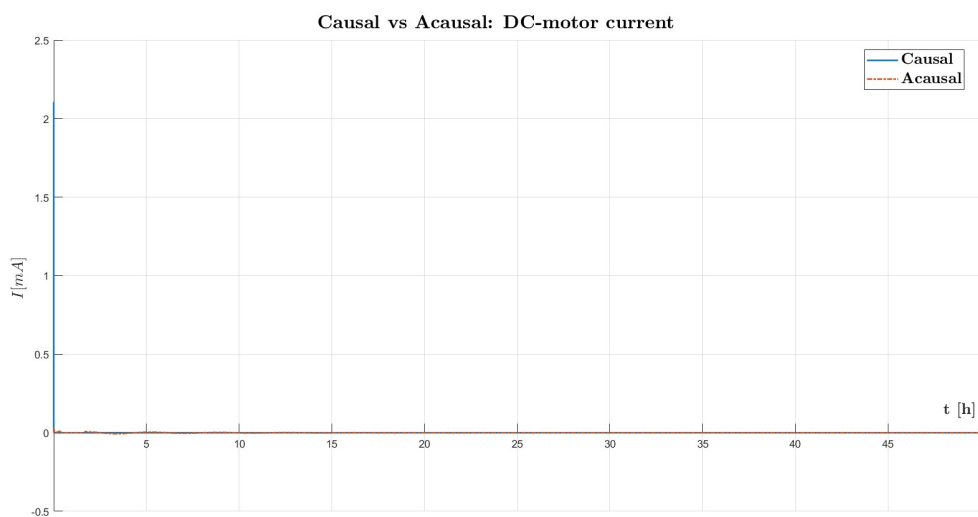


Figure 53: Causal vs Acausal: DC motor current

1.2 Exercise 2

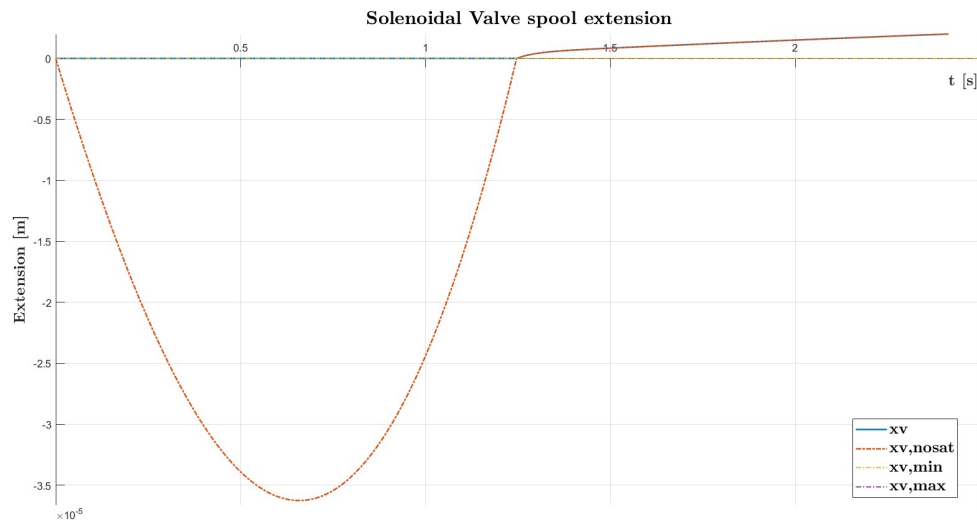


Figure 54: Acausal Spool extension evolution with and without Saturation block

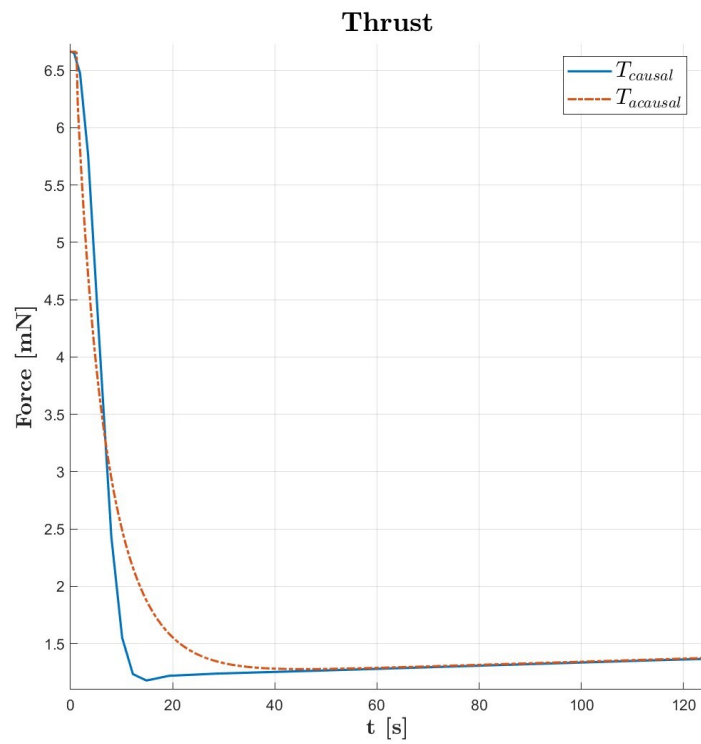
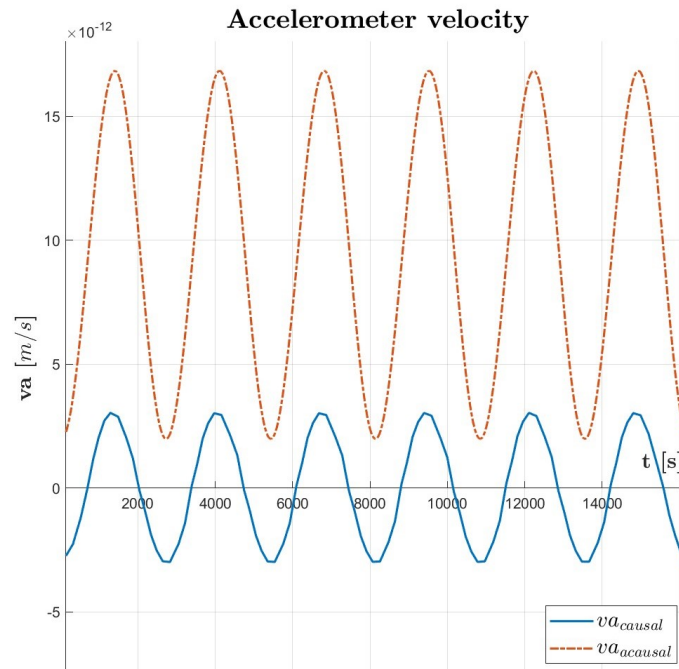
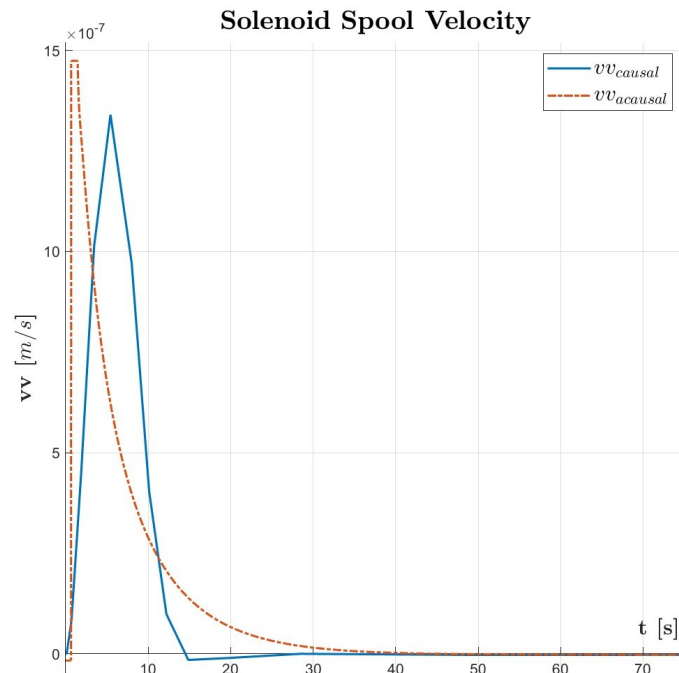


Figure 55: causal vs acausal: zoom on thrust evolution

**Figure 56:** causal vs acausal: zoom on v_a evolution**Figure 57:** causal vs acausal: zoom on v_v evolution

References

- [1] R. Mukhiya, M. Garg, P. Gaikwad, et al. *Electrical equivalent modeling of MEMS differential capacitive accelerometer*. In: Microelectronics Journal. Vol. 99, pp. 104770, 2020. <https://doi.org/10.1016/j.mejo.2020.104770>